The AMIGA sample of isolated galaxies. III. IRAS data and infrared diagnostics

Ute Lisenfeld, L. Verdes-Montenegro, Jack W. Sulentic, Sylvie Léon, D. Espada, Gilles Bergond, E. Garciá, J. Sabater, J. D. Santander-Vela, Simon Verley

A&A 462, 507–523 (2007)
DOI: 10.1051/0004-6361:20066144

Astronomy & Astrophysics

The AMIGA sample of isolated galaxies

III. IRAS data and infrared diagnostics⋆

U. Lisenfeld[1,2], L. Verdes-Montenegro[2], J. Sulentic[3], S. Leon[4], D. Espada[2], G. Bergond[2,5], E. García[2], J. Sabater[2], J. D. Santander-Vela[2], and S. Verley[2,6,7]

[1] Departamento de Física Teórica y del Cosmos, Facultad de Ciencias, Universidad de Granada, Spain
e-mail: ute@ugr.es
[2] Instituto de Astrofísica de Andalucía (IAA/CSIC), Apdo. 3004, 18080 Granada, Spain
[3] Department of Astronomy, University of Alabama, Tuscaloosa, USA
[4] Instituto de Radioastronomía Milimétrica (IRAM), Avda. Divina Pastora 7, local 20, 18012 Granada, Spain
[5] GEPI/CAI, Observatoire de Paris, 77 avenue Denfert-Rochereau, 75014 Paris, France
[6] LERMA - Observatoire de Paris, 61 avenue de l'Observatoire, 75014 Paris, France
[7] INAF-Osservatorio Astrofisico di Arcetri, Largo E. Fermi 5, 50125 Firenze, Italy

Received 31 July 2006 / Accepted 26 September 2006

ABSTRACT

Aims. We describe the mid- (MIR) and far- (FIR) infrared properties of a large (∼1000) sample of the most isolated galaxies in the local Universe. This sample is intended as a "nurture-free" zero point against which more environmentally influenced samples can be compared.

Methods. We reprocess IRAS MIR/FIR survey data using the ADDSCAN/SCANPI utility for 1030 out of 1050 galaxies from the Catalogue of Isolated Galaxies (CIG) as part of the AMIGA project. We focus on diagnostics (FIR luminosity $L_{\rm FIR}$, $R = \log(L_{\rm FIR}/L_B)$, and IRAS colours) thought to be sensitive to effects of environment or interaction.

Results. The distribution of $\log(L_{\rm FIR})$ sharply peaks from 9.0–10.5, with very few (<2%) galaxies above 10.5. Review of available optical images of the most FIR luminous galaxies finds the majority likely to be interacting systems missed in our earlier morphological reevaluation. The optically normalised luminosity diagnostic $R = \log(L_{\rm FIR}/L_B)$ shows a sharply peaked distribution between 0.0 and −1.0. These results were compared to the magnitude limited sample of the Center for Astrophysics that was selected without environmental discrimination. This modestly (e.g., compared to cluster, binary galaxy, and compact group samples) environmentally affected sample shows a significantly higher mean $\log(L_{\rm FIR})$, and R, whereas the mean $\log(L_B)$ is the same. Our sample shows a strong $L_{\rm FIR}$ vs. L_B correlation, with a slope steeper than one ($L_{\rm FIR} \propto L_B^{1.41}$). Interacting galaxies were found above this correlation, showing an enhancement in $L_{\rm FIR}$. With respect to the IRAS colours, we found higher F_{60}/F_{100} values for ellipticals and late-type galaxies than for spirals, indicating a higher dust temperature. The mean value of F_{60}/F_{100} was found to be lower than for interacting samples from the literature.

Conclusions. The results indicate that the FIR emission is a variable enhanced by interaction, and that our sample probably shows the lowest possible mean value. This attests to the utility of our sample for defining a nurture-free zero point.

Key words. galaxies: evolution – galaxies: interactions – galaxies: luminosity function, mass function – surveys – infrared: galaxies

1. Introduction

Although it is widely accepted that galaxy interactions *can* stimulate secular evolutionary effects in galaxies (e.g., enhanced star formation, morphological peculiarities including transitions to earlier type, active nuclei) (e.g., Sulentic 1976; Hernquist 1989; Xu & Sulentic 1991), there are still many open questions. Studies aimed at quantifying the level of interaction enhancement have even produced contradictory results; e.g., some studies of interacting pairs find a clear star formation enhancement (Bushouse et al. 1987; Bushouse 1988), while others find only a marginal increase (Bergvall et al. 2003). Much of this uncertainty reflects the lack of a statistically useful baseline. What is the amplitude and dispersion in a given galaxy property that can be ascribed to "nature"? A definition of "isolated galaxy" is needed before one can properly assess the history and properties of non-isolated ones. This has motivated us to build a well-defined and statistically significant sample of isolated galaxies to serve as a control sample for the study of galaxies in denser environments.

The AMIGA project (Analysis of the interstellar Medium of Isolated GAlaxies) involves the identification and study of a statistically significant sample of the most isolated galaxies in the local Universe. Our goal is to quantify the properties of different phases of the interstellar medium in these galaxies which are likely to be least affected by their external environment. We adopted the Catalogue of Isolated Galaxies (CIG: Karachentseva 1973; Karachentseva et al. 1986), including 1051 objects, as a base sample. All CIG galaxies are part of the Catalogue of Galaxies and Clusters of Galaxies providing reasonably uniform apparent magnitude measures (CGCG: Zwicky et al. 1961–1968) with $m_{\rm pg} < 15.7$ and $\delta > -3$ deg. Redshifts are now virtually complete for this sample with only

⋆ Full Tables 2 and 3 are available in electronic form at the CDS via anonymous ftp to
cdsarc.u-strasbg.fr (130.79.128.5) or via
http://cdsweb.u-strasbg.fr/cgi-bin/qcat?J/A+A/462/507
and from http://www.iaa.es/AMIGA.html

one of the compiled objects recognised as a Galactic source (CIG 781 ≡ Pal 15; Nilson 1973), reducing the working sample to $n = 1050$ objects. AMIGA is compiling data that will characterise all phases of the ISM: blue magnitude, mid- and far-infrared, Hα, and radio continuum fluxes, as well as the emission of the atomic gas (HI) and of carbon monoxide (CO), as a tracer of the molecular gas. The data are being released and periodically updated at `http://www.iaa.es/AMIGA.html`

Previous AMIGA papers evaluated, refined, and improved the sample in different ways including: 1) revised positions (Leon & Verdes-Montenegro 2003), 2) sample redefinition, magnitude correction, and full-sample analysis of the Optical Luminosity Function (OLF) (Verdes-Montenegro et al. 2005: Paper I), and 3) morphological revision and type-specific OLF analysis (Sulentic et al. 2006: Paper II). In the present paper we analyse basic mid- (MIR) and far-infrared (FIR) properties using data from the IRAS survey (Sects. 2 and 3). In Sect. 4 of the paper we present the FIR luminosity function followed by consideration of various MIR and FIR diagnostics that have been used in the past to quantify the effects of environment. In Sect. 5 we discuss the results and compare them to other studies. Future papers will present a quantification of the isolation condition and the analysis of the radio continuum, Hα, CO and HI data.

2. ADDSCAN/SCANPI analysis of the IRAS data

We present co-added ADDSCAN/SCANPI derived fluxes or upper limits for 1030 AMIGA galaxies. The remaining 20 galaxies in our sample were not covered by the IRAS survey. Previous studies involving CIG galaxies worked with smaller subsamples and, in most cases, used IRAS data from the Point Source (PSC) and Faint Source Catalogues (FSC). A subsample of 476 CIG galaxies with redshifts and PSC fluxes were used as a control sample for a study of FIR emission from isolated pairs (Xu & Sulentic 1991, hereafter XS91). Verdes-Montenegro et al. (1998) constructed a reference sample of 68 CIG galaxies with redshift and blue luminosity distributions matching their target set of Hickson (1982) compact groups. Hernandez-Toledo et al. (1999) obtained SCANPI data for 465 CIG galaxies (those with available redshift data) to use them as a reference in a study of galaxy pairs. FIR data for the CIG galaxies were, however, not published in that paper.

IRAS PSC and FSC data exist for only about half of the galaxies in our sample, motivating us to ADDSCAN/SCANPI reprocess our entire sample. We used the revised positions from Leon & Verdes-Montenegro (2003), which have a precision of 0.″5. ADDSCAN/SCANPI, a utility provided by the Infrared Processing and Analysis Center (IPAC) (`http://scanpi.ipac.caltech.edu:9000/`), is a one-dimensional tool that coadds calibrated IRAS survey data. It makes use of all scans that passed over a specific position and produces a scan spectrum along the average scan direction. It is 3–5 times more sensitive than IRAS PSC since it combines all survey data (Helou et al. 1988) and is therefore more suitable for detection of the total flux from slightly extended objects. Our sample was well suited for ADDSCAN/SCANPI processing because: i) confusion is minimised since our sample galaxies were selected with an isolation criterion and ii) the galaxies are small enough to permit derivation of reliable fluxes. An analysis of the IRAS Bright Galaxy Sample (BGS) with ADDSCAN/SCANPI (Sanders et al. 2003) found that missed flux became important only for optical sizes larger than 25′. About 97% of the galaxies in our sample are smaller than 4′.

Table 1. Detection rates and point vs. extended source numbers for the CIG IRAS sample ($n = 1030$).

λ	Threshold	Detections	Detection rate	Extended	Point
12	3σ	180	17%	40	141
	5σ	94	9%	37	57
25	3σ	245	24%	57	188
	5σ	158	15%	53	105
60	3σ	729	71%	84	645
	5σ	591	57%	82	509
100	3σ	673	65%	37	636
	5σ	526	51%	36	491

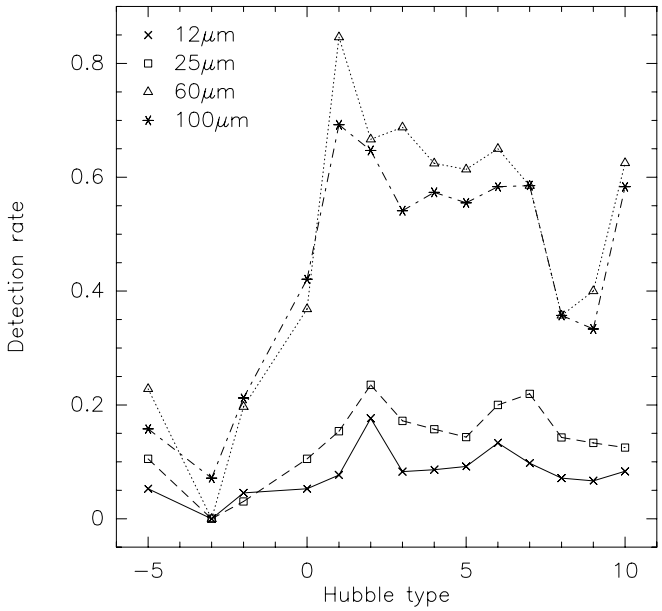

Fig. 1. Detection rate at 12, 25, 60, and 100 μm as a function of Hubble type.

ADDSCAN/SCANPI derives four different flux estimators: a) *Peak*: maximum flux density within the signal range specified, b) *fnu*(z): total flux density estimated from integration of the averaged scan between the zero crossings, c) *Templ*: flux density estimated from the best-fitting point source template, and d) *fnu*(t): total flux density estimated from integration of the averaged scan between fixed points defining an integration range. We adopted the default SCANPI ranges (corresponding to the nominal IRAS detector size) [−2′, +2′], [−2′, +2′], [−2.′5, +2.′5], and [−4′, +4′] at 12, 25, 60, and 100 μm, respectively. We used the median as the most robust combination of scans and followed IPAC indications to choose the best flux density from among the estimators for each galaxy. We first flagged those galaxies with a $S/N > 3$ as detected. We visually confirmed all cases and found some errors produced by bright stars in the field or baseline corruption from noise or cirrus.

Table 1 summarises the number of detected sources at each IRAS band. For completeness, we also include the corresponding numbers for a detection threshold of 5 times the rms noise level, which is the limit used in the data analysis carried out in this paper (see Sect. 4.1). Figure 1 shows the detection rate (at a 3σ detection threshold) at the four IRAS wavelengths as a function of Hubble type. The MIR-FIR detection rates show a minimum for early-type galaxies gradually increasing from 10−20% to 20−80% for late-type spirals. We see a decline to 20−60%

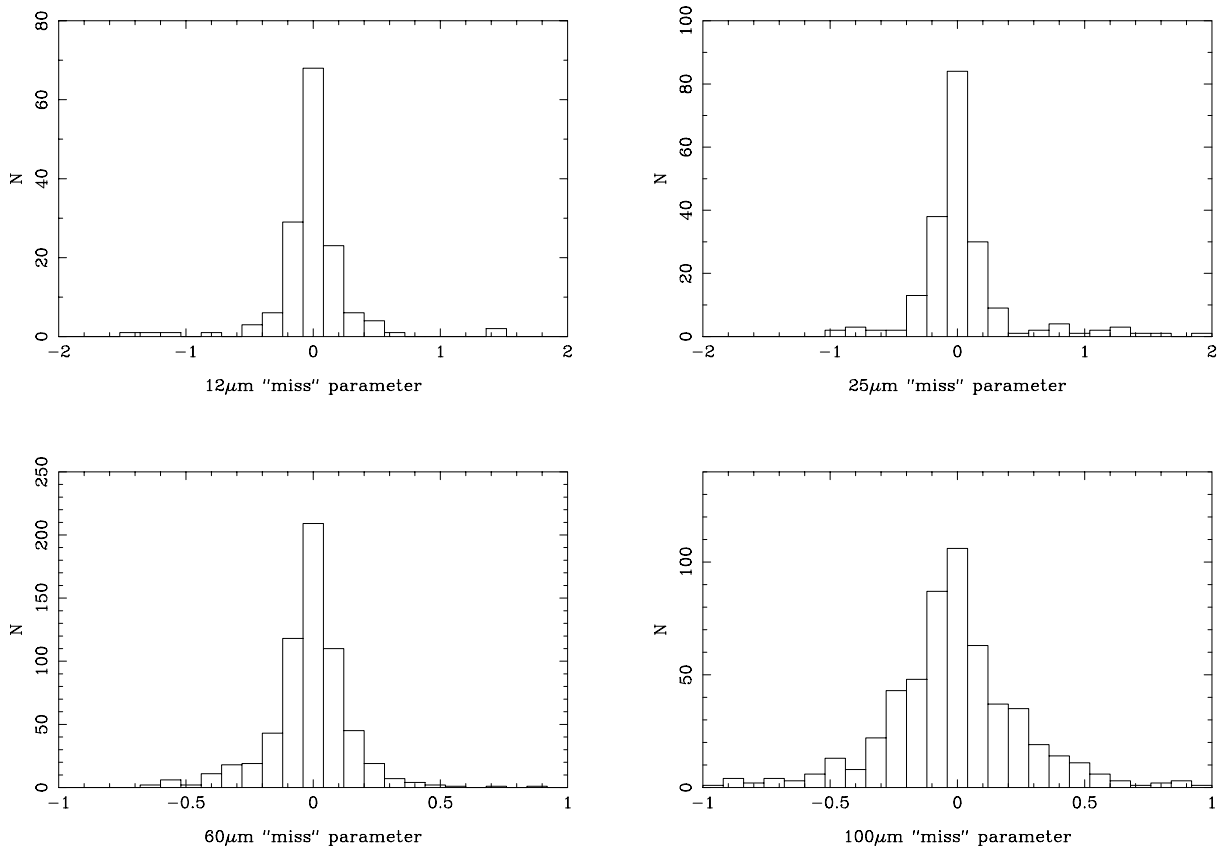

Fig. 2. Histogram of the "miss" parameter (offset in arcmin between the galaxy position and the position of the signal peak) for each IRAS band.

beyond type Sd ($T = 7$), probably reflecting an increasing dwarf galaxy population with low dust masses.

Figure 2 plots the "miss" parameter, which is the offset in arcmin between the galaxy position and the position of the signal peak along the average scan direction. This parameter is used as the primary measure of source identification. The majority of sources cluster around zero offset with the largest deviations occurring at 12 and 25 μm because: 1) the resolution is higher and 2) the S/N is usually lower than at longer wavelengths. The standard deviations of the "miss" parameter are 18″, 24″, 14″ and 28″, respectively, for 12, 25, 60, and 100 μm. This is a factor of $\frac{1}{2}$ to $\frac{1}{6}$ of the nominal *FWHM* of the IRAS detectors (0.′77, 0.′78, 1.′44, and 2.′94 at 12, 25, 60, and 100 μm respectively). This scatter is reasonable when one allows for the fact that most of these galaxies are not very infrared (IR) bright so that determination of the source centroid depends somewhat on the S/N of the measurement.

In the next step we used two different tests to decide whether a detected source was extended or pointlike with respect to the IRAS beam. In Test 1 we considered those galaxies where the signal width was greater than the expected width for a point source as extended. We used both *w25* and *w50* (width of the signal in arcminutes at 25% and 50% peak) for this comparison. We compared our measures to the widths of point sources (Sanders et al. 2003), where *w25psf* and *w50psf* were 1.′40, 1.′38, 2.′06, and 4.′32, and 1.′04, 1.′00, 1.′52, and 3.′22 at 12, 25, 60, and 100 μm, respectively. In Test 2 we classified those sources where the integrated flux, *fnu*(z), was substantially larger than the peak flux as extended, adopting the condition *fnu*(z) − *Peak* > 5σ as a threshold criterion for an extended source. The percentages of galaxies showing conflicting classifications in the two tests were 9, 17, 23, and 18% at 12, 25, 60, and 100 μm, respectively. We revised these cases interactively and found the differences were most often due to baseline corruption by noise and/or cirrus. Table 1 lists the number of sources classified as point or extended for each IRAS band. The 5σ cutoff reduces, compared to the 3σ cutoff, mainly the number of detected point sources and leaves the number of detected extended sources almost unchanged. The reason is that sources classified as extended have $S/N > 5$ in most cases. Once the size of a source was decided we could choose a flux estimator following guidelines given by IPAC. For point sources, three cases were considered: a) if *Templ* > 20 Jy we used *Peak*, b) if *Templ* < 1 Jy (<2 Jy at 100 μm) we used *Templ*, and c) if 1 Jy < *Templ* < 20 Jy (2 Jy < *Templ* < 20 Jy at 100 μm) we used *Templ* if *Peak* and *fnu*(t) agreed within 3σ. Otherwise we visually determined the best estimator of the total flux density. In the case of extended sources we used *fnu*(z) when $S/N > 10$ and *fnu*(t) for the rest.

3. The data

Table 2 lists λ 12, 25, 60, and 100 μm derived fluxes obtained using procedures explained in Sect. 2. We also tabulate some related parameters, as detailed in the notes to the table.

3.1. Comparison to other IRAS catalogues

We compared IRAS fluxes obtained with SCANPI to data available from the IPAC archives and in the literature. We retrieved data from the Faint Source Catalogue (FSC) and the Point Source Catalogue (PSC) from the IRAS database through the GATOR service (`http://irsa.ipac.caltech.edu/`). We found 509 CIG galaxies in the FSC and additional data

Table 2. FIR flux densities[1].

	12 μm				25 μm				60 μm				100 μm			
(1)	(2)	(3)	(4)	(5)	(6)	(7)	(8)	(9)	(10)	(11)	(12)	(13)	(14)	(15)	(16)	(17)
CIG	F_{12}	rms	M	E	F_{25}	rms	M	E	F_{60}	rms	M	E	F_{100}	rms	M	E
	(Jy)	(Jy)			(Jy)	(Jy)			(Jy)	(Jy)			(Jy)	(Jy)		
1	<0.07	0.02	5		<0.23	0.08	5		0.86	0.07	1	n	2.87	0.16	2	n
2	<0.09	0.03	5		<0.11	0.04	5		0.21	0.05	1	n	0.74	0.21	1	n
3	0.06	0.02	1	n	<0.08	0.03	5		0.19	0.03	1	n	0.43	0.07	1	n
4	0.66	0.03	4	y	0.61	0.03	4	y	5.19	0.05	4	y	16.78	0.12	4	y
5	<0.13	0.04	5		0.12	0.04	2	n	0.25	0.04	1	n	0.76	0.14	1	n
...	...	...	...	...	...	...	...	...	...	...	...	...	...	...	...	...

The table format is: *Column 1*: CIG number. *Column 2*: Flux density at 12 μm, calculated as explained in Sect. 2. Upper limits are preceded by a "<" sign. A 3σ value has been adopted for the upper limits, except for CIG 397 where the 12 μm scan presents confusion with a close star and 20% of the peak of the emission has been adopted as an upper limit. *Column 3*: rms noise of the data at 12 μm. *Column 4*: method used to derive the flux densities given in Col. 2. Codes 1 to 4 correspond to the following flux estimators: 1 = *Templ*, 2 = *Peak*, 3 = *fnu*(t), and 4 = *fnu*(z). Code 5 corresponds to upper limits obtained as 3σ. Code 6 is reserved for some particular cases: CIG 397 (see above) and nine galaxies included in the catalogue of large optical galaxies of Rice et al. (1988) (CIG 105, 197, 324, 347, 461, 469, 523, 559 and 610) where we have used the values given in their catalogue (see also Sect. 3.1). *Column 5*: detected galaxies are flagged with "y" if they have been classified as extended, and with "n" when classified as point sources. *Columns 6–9*: the same as Cols. 2–5 for 25 μm. *Columns 10–13*: the same as Cols. 2–5 for 60 μm. *Columns 14–17*: the same as Cols. 2–5 for 100 μm.

[1] The full table is available in electronic form at the CDS and from `http://www.iaa.es/AMIGA.html`

for 15 galaxies in the PSC. The average error-weighted ratios F(SCANPI)/F(FSC+PSC) for galaxies detected both by SCANPI and in the FSC+PSC are 1.24 ± 0.50 (n = 114), 1.16 ± 0.33 (n = 153), 1.09 ± 0.15 (n = 501), and 1.05 ± 0.13 (n = 407) for 12, 25, 60, and 100 μm. The average ratio is slightly larger than one and decreases with increasing wavelength. This indicates that the flux derivation with SCANPI is able to pick up more flux for extended objects than FSC/PSC, especially at short wavelengths where the IRAS beam is smaller. There is a large number of galaxies with FSC/PSC tabulated upper-limits (n = 55, 70, 9, and 81 for 12, 25, 60 and 100 μm) that were replaced by SCANPI detections indicating that the detection rate has been improved by the reprocessing. Other galaxies were listed as FSC/PSC detections while SCANPI derived only upper limits (n = 29, 21, 5, and 3 for 12, 25, 60 and 100 μm). We checked those cases individually and found that all were weak sources where either: 1) the automated SCANPI procedure did not confirm a detection or 2) we decided, after visual inspection, that $S/N < 3$.

Figure 3 shows the SCANPI-to-FSC/PSC flux ratio as a function of optical diameter for each IRAS band. We exclude detections where SCANPI and FSC/PSC fluxes agree within the uncertainties (which is the case for 82, 107, 397 and 368 galaxies at 12, 25, 60 and 100 μm, respectively). The 12 and 25 μm plots, and to a lesser extent 60 μm, show that F(SCANPI)/F(FSC+PSC) increases with optical diameter above about 1′–3′. This supports our inference that FSC/PSC flux densities are often underestimated for large galaxies because part of the flux falls outside the IRAS beam and that SCANPI is able to provide a more realistic flux estimate for these sources. There are only three galaxies (CIG 546, 616 and 721) with F(SCANPI)/F(FSC+PSC) significantly below one. In the case of CIG 546 (F_{60}(SCANPI)/F_{60}(FSC+PSC) = 0.66) and CIG 721 (F_{60}(SCANPI)/F_{60}(FSC+PSC) = 0.72), the origin of the difference is unclear since we have no reason to doubt the reliability of our SCANPI estimates. CIG 616 (F_{12}(SCANPI)/F_{12}(FSC+PSC) = 0.56) was detected by SCANPI just above a 3σ level so that the flux density has a larger uncertainty.

We compared 18 galaxies in common with the Bright IRAS Galaxy sample (F_{60} > 5.24 Jy), where flux densities were also derived using SCANPI (Sanders et al. 2003). Agreement is better than 6% for all sources at 12, 60, and 100 μm. At 25 μm there are three sources (CIG 442, 549, and 1004), where our adopted values exceed those derived by Sanders et al. (2003) at the 10−20% level. We think that the discrepancy arises because some of the flux in these sources extends beyond the integration range used in deriving *fnu*(t) and will therefore be better estimated using our *fnu*(z) values.

Following IPAC recommendations, we compared the results derived with SCANPI to those derived from 2D Full Resolution Coadded (FRESCO) images for sources with optical diameter larger than 2.′5 (107 objects). Since FRESCO images do not have the large-scale background removed (they are not point-source filtered), they provide additional information about galaxy environments including possible confusion due to nearby stars or Galactic cirrus. We extracted individual source fluxes from FRESCO images using Sextractor (Bertin & Arnouts 1996). We extracted fluxes for CIG galaxies using both 3 and 5σ thresholds above the local background level to estimate the effects of background and particularly Galactic cirrus. Calibrated FRESCO fluxes for the 4 IRAS bands were compared to the SCANPI fluxes, and we found ratios F(SCANPI)/F(FRESCO) close to unity (1.04 ± 0.42, 0.98 ± 0.40, 0.89 ± 0.33 and 0.97 ± 0.44 at 12, 25, 60 and 100 μm), respectively. Scatter was high, but we did not find a trend with optical diameter that might point towards flux being missed using either procedure. It is more likely that contamination from the local foreground (Galactic emission) dominates the flux determination.

Finally, we searched for CIG galaxies included in the catalogue of large optical galaxies (Rice et al. 1988) and found nine objects (CIG 105, 197, 324, 347, 461, 469, 523, 559, and 610). In most cases we find reasonable (within 2σ) agreement between flux estimates. There are some significant discrepancies for the largest objects. The most severe discrepancy involves the galaxy with the largest apparent optical diameter CIG 610 (≡M 101, 28.′8 × 26.′9), where SCANPI fluxes are only 10−35% of the fluxes given in Rice et al. (1988). Disagreements of up to a factor of 2.5 are present for CIG 197 (≡NGC 2403, 21.′9 × 12.′3) and CIG 523 (≡NGC 4236, 21.9′ × 7.2′). The single discrepancy involving a smaller galaxy, CIG 105 (≡NGC 925, 10.′5 × 5.′9), finds a SCANPI flux at 12 μm that is almost a factor of two lower

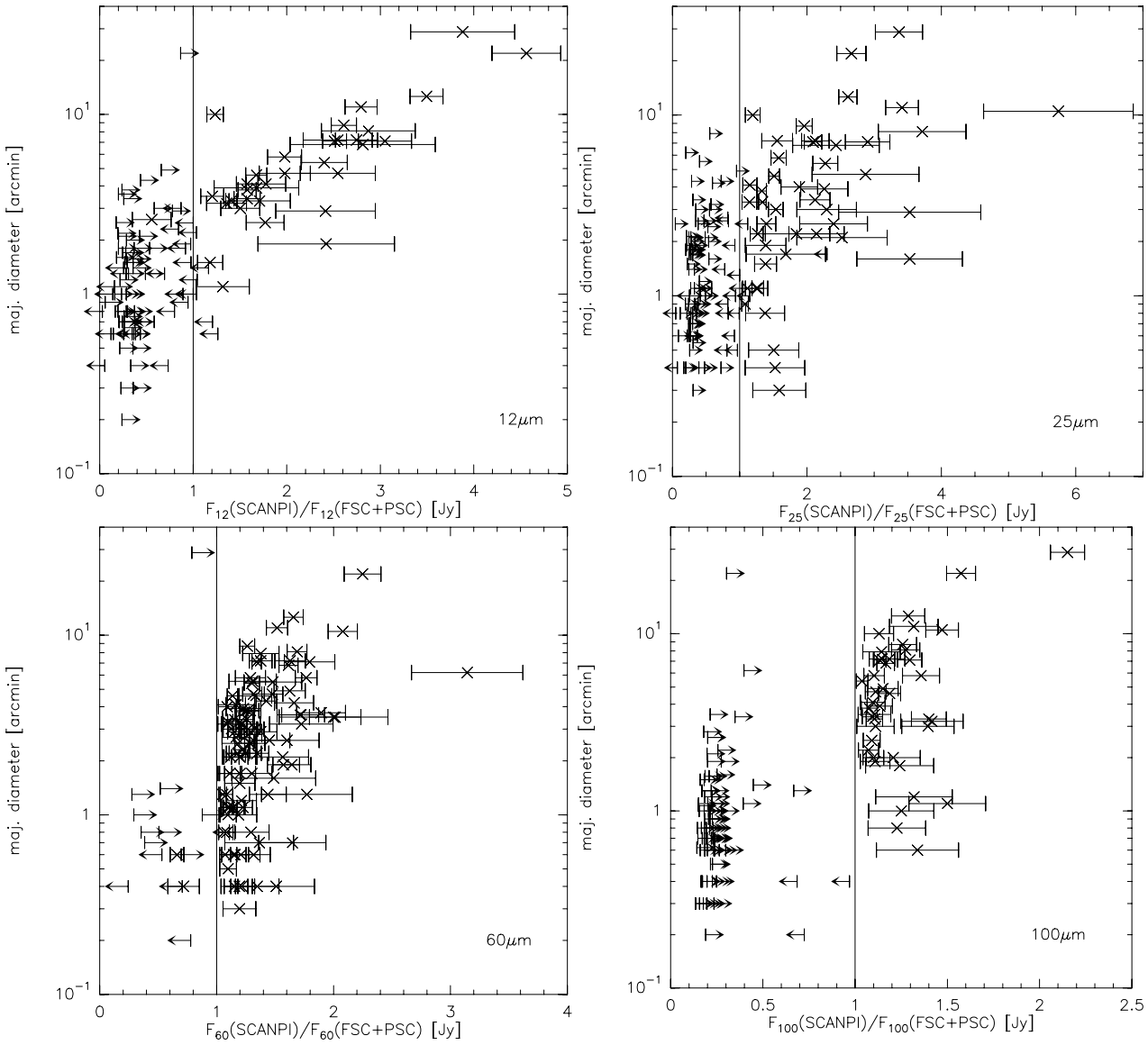

Fig. 3. SCANPI/FSC+PSC flux ratio as a function of optical diameter for the 4 IRAS wavelengths. Detected galaxies showing consistent fluxes between SCANPI and FSC+PSC are not included in the figure for clarity.

than the flux in Rice et al. (1988). We adopted the flux densities of Rice et al. (1988) for all nine galaxies.

4. Data analysis

4.1. Sample definition

In the following sections we analyse the FIR emission properties of the CIG galaxy sample. To do this in a statistically meaningful way, we focus on the optically complete sample described in Paper I. This sample involves galaxies with corrected Zwicky magnitudes in the range 11.0–15.0 for which we found $\langle V/V_m \rangle = 0.40$, indicating 80% completeness. We include some changes/upgrades with respect to the previously defined sample (in Paper I) in the present work:

1. We include 20 galaxies for which redshift information has become available since the publication of Paper I (the updated redshift list is available from `http://www.iaa.es/AMIGA.html`).
2. Morphological revision of the sample, described in Paper II, identified 32 galaxies that are probably not isolated in the sense that they might involve isolated interacting pairs and/or multiplets. These galaxies are excluded from the most isolated sample and represent part of the AMIGA refinement. However they provide us with a useful internal comparison sample to test the effects of interaction contamination.
3. We recomputed corrections to the Zwicky magnitudes following Paper I, but using the revised morphologies from Paper II. This change in individual magnitudes will therefore slightly change the sample involving galaxies in the range 11.0–15.0 mag. The present sample shows a value of $\langle V/V_m \rangle = 0.43$, indicating a slightly improved level of completeness compared to Paper I.
4. We exclude two nearby dwarf ellipticals (CIG 663 ≡ Ursa Minor and CIG 802 ≡ Draco) for which we have only IRAS upper limits and very low inferred luminosity limits ($\log(L_{\rm FIR}/L_\odot) < 3.25$).

We are left with a sample of 719 galaxies with IRAS data, and redshift data is available for 701 galaxies of them. Hereafter we

Table 3. FIR and blue luminosities[1].

(1) CIG	(2) Distance (Mpc)	(3) $\log(L_{\rm FIR})$ $(L_\odot)$	(4) $\log(L_B)$ $(L_\odot)$
1	92.2	10.23	10.44
2	88.7	< 9.72	9.76
3	–	–	–
4	26.1	9.91	10.17
5	100.2	9.75	10.07
...	...	...	

The entries are: *Column 1*: CIG number. *Column 2*: distance in Mpc from Paper I. *Column 3*: FIR luminosity, calculated as described in Sect. 4.2. Upper limits are indicated with < in front of the value. Galaxies with distances, but without FIR data points (in total: 20 objects) lie in the area not covered by IRAS. *Column 4*: blue luminosity, calculated as described in Sect. 4.4.
[1] The full table is available in electronic form at the CDS and from `http://www.iaa.es/AMIGA.html`

will refer to this sample as the AMIGA (FIR) sample. We decided to increase the detection threshold to 5σ to make sure that we only consider reliable detections. Thus, with respect to Table 2, we now consider only those fluxes as detections where the S/N ratio is above 5, and we use an upper limit of 5 times the rms noise for values below. (We chose to leave the 3σ detection limit in Table 2 to provide the complete data set.) With this higher threshold, 511 galaxies have a detection at least at one wavelength. This sample can be cut in many different ways. Right now we make no restriction in recession velocity. This allows us to sample the widest possible luminosity range. Sources with $V \leq 1500$ km s^{-1} provide an insight into the IR emission from local dwarf galaxies that are not included in the rest/bulk of the sample. The drawback about including these galaxies in the sample involves the difficulty in reliably assessing their isolation properties.

4.2. FIR luminosity

FIR luminosity, $L_{\rm FIR}$, is computed from IRAS measurements as $\log(L_{\rm FIR}/L_\odot) = \log({\rm FIR}) + 2\log(D) + 19.495$, where D is distance in Mpc and $FIR = 1.26 \times 10^{-14}(2.58F_{60} + F_{100})$ W m^{-2} (Helou et al. 1988) the flux in the FIR range, with the IRAS fluxes at 60 and 100 μm, F_{60} and F_{100}. $L_{\rm FIR}$ and the distances adopted are listed in Table 3.

Figure 4 shows the distribution of FIR luminosity for the optically complete AMIGA sample, and the mean and median values are given in Table 4. In Fig. 4, we include individual histograms for: 1) galaxies detected at both 60 and 100 μm, 2) those not detected at one or both wavelengths and 3) the distribution calculated using survival analysis that takes upper limits into account. We use the ASURV package for the latter calculations throughout this paper[1]. The distribution peaks in the bin $\log(L_{\rm FIR}/L_\odot) = 9.5$–$9.75$ with the ASURV estimated mean $\log(L_{\rm FIR}/L_\odot) = 9.15$ (see Table 4). Practically all galaxies have FIR luminosities between $\log(L_{\rm FIR}/L_\odot) = 7.5$ and $\log(L_{\rm FIR}/L_\odot) = 11.25$. Only one object, the faint irregular member of the Local Group CIG 388 (≡Sextans B), shows

[1] Astronomy Survival Analysis (ASURV) Rev. 1.1 is a generalised statistical package that implements the methods presented by Feigelson & Nelson (1985) and Isobe et al. (1986), and is described in detail in Isobe & Feigelson (1990) and La Valley et al. (1992).

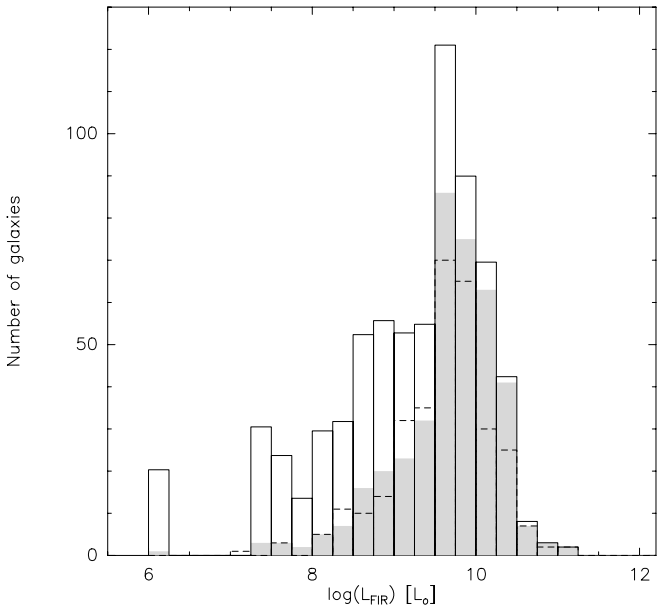

Fig. 4. The FIR luminosity distribution of the optically selected sample described in Sect. 4.1. The full line shows the distribution calculated with ASURV ($n = 701$), the shaded area shows all galaxies detected at both 60 and 100 μm ($n = 478$), and the dashed line gives the non-detections.

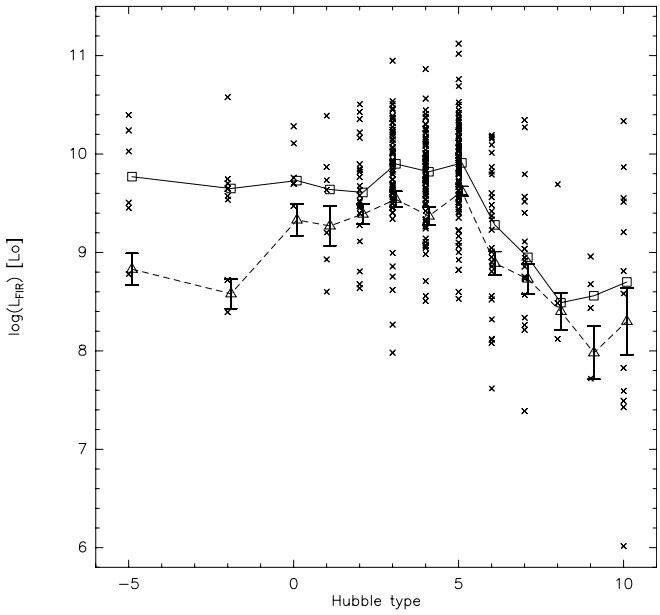

Fig. 5. Distribution of FIR luminosity as a function of Hubble type. Only detections are shown. The open triangles give the mean value for each Hubble type, calculated with ASURV and taking the upper limits into account. The open squares are the median values for the detections only.

$\log(L_{\rm FIR}/L_\odot) = 6.01$. It is remarkable that the bulk of the FIR luminosities (98%) lies below $\log(L_{\rm FIR}/L_\odot) = 10.5$.

In Fig. 5 we show the distribution of the FIR luminosities as a function of Hubble type, and in Fig. 4 we list the mean (taking upper limits into account with ASURV) and median (for detections only) values. The mean values show a strong increase after the early types (E−S0) beginning at $T = 0$ (S0a) and increasing through $T = 5$ (Sc), followed by a decline to a near constant mean for the latest types ($T = 8$–10). ASURV means for

Table 4. Mean and median values of $L_{\rm FIR}$, L_B, and $R = \log(L_{\rm FIR}/L_B)$.

(1) Sample	(2) n	(3) $\langle\log(L_B)\rangle$ med($\log(L_B)$)	(4) $n_{\rm up}$	(5) $\langle\log(L_{\rm FIR})\rangle$ med($\log(L_{\rm FIR})$)	(6) n	(7) $n_{\rm up}$	(8) $\langle R\rangle$ med(R)
Total	701	9.97 ± 0.02	312	9.15 ± 0.06	719	327	−0.56 ± 0.03
		10.06		9.74			−0.29
S/Im (T = 1–10)	616	9.98 ± 0.02	248	9.26 ± 0.05	634	263	−0.49 ± 0.02
		10.07		9.76			−0.30
E (T = −5)	27	9.95 ± 0.06	21	8.83 ± 0.16	27	21	−1.01 ± 0.12
		10.01		9.77			−0.14
S0 (T = −2)	36	9.82 ± 0.08	27	8.58 ± 0.15	36	27	−0.95 ± 0.09
		9.95		9.65			−0.23
S0a (T = 0)	14	9.88 ± 0.07	8	9.33 ± 0.16	14	8	−0.57 ± 0.15
		9.88		9.73			−0.03
Sa (T = 1)	10	9.92 ± 0.18	3	9.27 ± 0.20	10	3	−0.60 ± 0.10
		10.00		9.64			−0.49
Sab (T = 2)	39	10.05 ± 0.05	15	9.39 ± 0.10	39	15	−0.62 ± 0.08
		10.00		9.61			−0.29
Sb (T = 3)	115	10.06 ± 0.04	42	9.54 ± 0.08	118	45	−0.38 ± 0.04
		10.10		9.90			−0.14
Sbc (T = 4)	155	10.10 ± 0.03	70	9.37 ± 0.09	160	73	−0.50 ± 0.03
		10.15		9.82			−0.32
Sc (T = 5)	182	10.12 ± 0.03	69	9.62 ± 0.05	188	74	−0.38 ± 0.02
		10.20		9.91			−0.28
Scd (T = 6)	47	9.65 ± 0.08	19	8.89 ± 0.12	47	19	−0.54 ± 0.06
		9.77		9.28			−0.35
Sd (T = 7)	34	9.58 ± 0.09	15	8.73 ± 0.15	38	19	−0.64 ± 0.06
		9.51		8.95			−0.52
Sdm(T = 8)	10	9.38 ± 0.21	7	8.40 ± 0.19	10	7	−0.55 ± 0.05
		9.05		8.49			−0.50
Sm (T = 9)	9	9.11 ± 0.34	5	7.98 ± 0.27	9	5	−0.58 ± 0.05
		9.07		8.56			−0.61
Im(T = 10)	15	9.01 ± 0.21	3	8.30 ± 0.34	15	3	−0.58 ± 0.13
		9.04		8.70			−0.47
Interacting	14	9.99 ± 0.11	2	9.87 ± 0.20	14	2	−0.06 ± 0.08
		9.98		10.02			−0.11

The entries are: *Column 1*: subsample considered. All subsamples are selected from the optically complete, magnitude limited subsample. The interacting subsample consists of the galaxies from the CIG excluded in Paper II (see Sect. 4.1). *Column 2*: total number of galaxies with velocity and IRAS data in the subsample. *Column 3*: first row: mean value of L_B. Second row: median value of L_B. *Column 4*: number of upper limits in FIR (at 60 or 100 μm). *Column 5*: first row: mean value of $L_{\rm FIR}$, using the Kaplan-Maier estimator from ASURV. Second row: median value of $L_{\rm FIR}$, only for detections. *Column 6*: total number of galaxies with IRAS data in the subsample. *Column 7*: number of upper limits in FIR (at 60 or 100 μm). *Column 8*: first row: mean value of $R = \log(L_{\rm FIR}/L_B)$, using the Kaplan-Maier estimator from ASURV. Second row: median value of R, only for detections.

early types are most strongly driven by upper limits with most detected E–S0 showing $L_{\rm FIR}$ values above the computed means, similar to those for late-type spirals. This marks the detections as unusual, indicating that these may not be typical (or even) E−S0 galaxies (see discussion in Paper II). As we proceed from left to right in the plot, the effect of upper limits gradually decreases and mean and median values converge. Our previously identified (Paper II) dominant (∼65%) isolated late-type (T = 3–5) spiral population shows FIR luminosities strongly concentrated (due to the minimisation of nurture-driven dispersion) in the range 9.4–10.5. We also observe a small but significant population of spiral types T = 2–7 with very low FIR luminosities. We see an apparent strong drop in mean FIR luminosity (∼0.7 in $\log(L_{\rm FIR})$) later than type T = 5. If real, there are three candidate explanations: 1) decreasing dust mass simply following decreasing galaxy mass for Scd–Sd, 2) decreasing dust content in Scd–Sd, or 3) less efficient star formation in Scd–Sd (always relative to Sb–Sc). The latest types show minimal upper limits since they are very local. This mostly dwarf galaxy population falls out of our magnitude limited sample beyond a few $\times 10^3$ km s^{-1} recession velocity.

4.3. FIR luminosity function

Since the AMIGA sample is optically selected we derive the FIR luminosity function (FIRLF) from the optical luminosity function and the fractional bivariate function between FIR luminosity and optical luminosity (see Paper I). The differential FIRLF, which gives the number density of galaxies per unit volume and per unit $\log(L_{\rm FIR})$ interval is derived from the following formula:

$$\Psi(L) = 2.5\Delta M \sum_j \Theta(L|M_j)\Phi(M_j), \quad (1)$$

where $L = \log(L_{\rm FIR})$, and Ψ is the differential FIRLF. The bivariate (optical, FIR) luminosity function $\Theta(L|M_j)$ is defined as

$$\Theta(L|M_j) = \frac{P(L, M_j)}{\Delta L}, \quad (2)$$

where $\Delta L = 0.25$ and $P(L, M_j)$ is the conditional probability for a source with absolute magnitude M ($M_j + 0.5\Delta M \geq M > M_j - 0.5\Delta M$) to have the logarithm of its FIR luminosity, $\log(L_{\rm FIR})$, within the interval $[L - 0.5\Delta L, L + 0.5\Delta L]$. The Kaplan-Meier

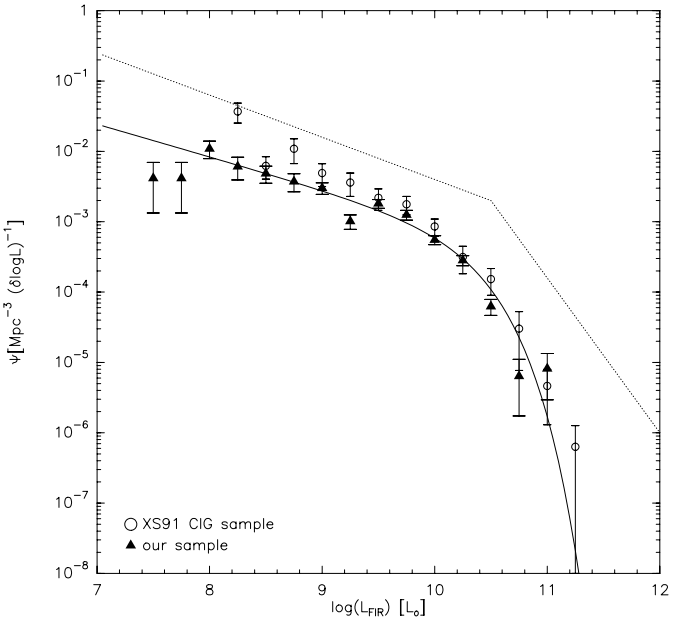

Fig. 6. Bivariate FIR luminosity function of our sample compared to the CIG sample used in XS91. The dotted line is the fit with a double power law derived in Sanders et al. (2003) for the Bright IRAS galaxy sample. The full line is a Schechter fit to our data.

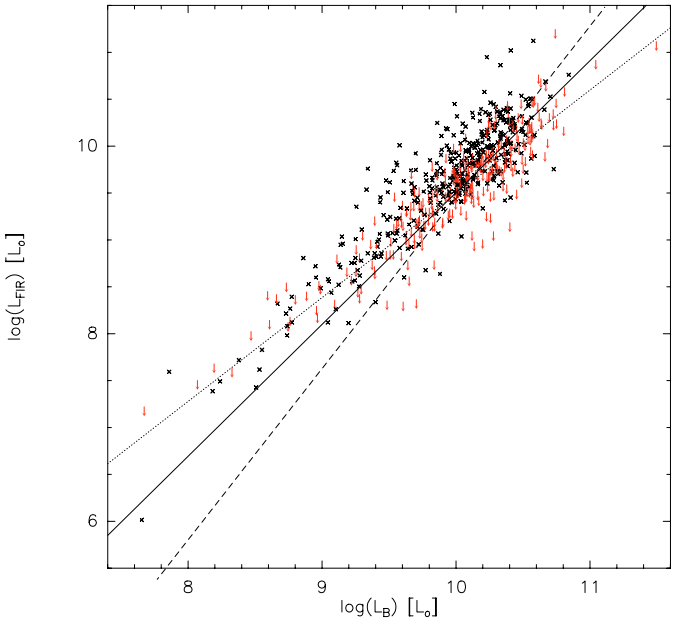

Fig. 7. $L_{\rm FIR}$ vs. L_B for the optically complete, magnitude limited subsample (n = 701, see Sect. 4.2 for exact definition). The full line indicates the best-fit bisector slope derived with ASURV, the dotted line shows the result of the regression adopting L_B, and the dashed line adopting $L_{\rm FIR}$ (dashed) as independent variable.

estimator (Schmitt 1985; Feigelson & Nelson 1985), which also exploits the information content of upper limits, has been used in computing the bivariate luminosity function and the associated errors. Φ is the differential OLF per unit volume and per unit magnitude interval, ΔM is the bin width of the OLF in magnitude units. The factor 2.5 arises because a unit magnitude interval corresponds to only 0.4 unit of L. The summation is over all bins of the OLF. The errors of $\Psi(L)$ are the quadratic sum of the uncertainties for the OLF and bivariate luminosity function.

Figure 6 shows the resultant FIRLF and Table 5 lists the corresponding values. Also shown is the FIRLF from XS91 for a smaller subsample of the CIG. We see that the general shape has not changed substantially with the use of a larger and more complete sample. It is our contention that it represents the best "natural" or "nurture-free" FIRLF yet derived. A strong decline in the FIRLF above $\log(L_{\rm FIR}/L_\odot) \sim 10.5$ is clearly visible. In the last few bins there are only very few objects (see Table 5), making the value of the FIRLF uncertain.

We have fitted the FIRLF with a Schechter function:

$$\Psi(L) = \Psi_0 \left(\frac{L}{L^\star}\right)^\alpha \exp\left(-\frac{L}{L^\star}\right). \quad (3)$$

The best-fit parameters are $\Psi_0 = (7.4 \pm 1.4) \times 10^{-4}$ Mpc^{-3} $(\delta \log(L_{\rm FIR}))^{-1}$, $L^\star = (1.9 \pm 0.2) \times 10^{10} L_\odot$, and $\alpha = -0.46 \pm 0.05$. We have also plotted the fit to the IRAS Bright Galaxy Sample FIRLF (Sanders et al. 2003) in Fig. 6. Sanders et al. (2003) found, in agreement with other FIR selected samples, that a double power law provides the best fit to the data. The difference from a Schechter fit typically starts to be noticeable above $10^{11} L_\odot$. Sulentic & Rabaca (1994) earlier pointed out the difficulty with using a Schechter function to adequately describe nurture-affected samples. With only three galaxies above $\log(L_{\rm FIR}/L_\odot) = 11.0$, our sample is well fit by a Schechter function.

Table 5. FIR luminosity function.

$\log(L_{\rm FIR})$ (in $L_\odot$)	Ψ (Mpc^{-3} log$(L)^{-1}$)	n
7.50	$4.15 \times 10^{-3} \pm 2.82 \times 10^{-3}$	2.5
7.75	$4.15 \times 10^{-3} \pm 2.82 \times 10^{-3}$	2.5
8.00	$1.09 \times 10^{-2} \pm 3.05 \times 10^{-3}$	19.6
8.25	$6.09 \times 10^{-3} \pm 2.17 \times 10^{-3}$	28.7
8.50	$4.85 \times 10^{-3} \pm 1.32 \times 10^{-3}$	23.0
8.75	$3.73 \times 10^{-3} \pm 1.07 \times 10^{-3}$	34.9
9.00	$3.01 \times 10^{-3} \pm 5.63 \times 10^{-4}$	101.2
9.25	$1.02 \times 10^{-3} \pm 2.35 \times 10^{-4}$	38.1
9.50	$1.81 \times 10^{-3} \pm 2.56 \times 10^{-4}$	123.9
9.75	$1.25 \times 10^{-3} \pm 1.98 \times 10^{-4}$	132.5
10.00	$5.51 \times 10^{-4} \pm 8.06 \times 10^{-5}$	95.5
10.25	$2.83 \times 10^{-4} \pm 4.60 \times 10^{-5}$	61.5
10.50	$6.26 \times 10^{-5} \pm 1.59 \times 10^{-5}$	21.0
10.75	$6.40 \times 10^{-6} \pm 4.66 \times 10^{-6}$	3.1
11.00	$8.17 \times 10^{-6} \pm 5.23 \times 10^{-6}$	3.0

The entries are: *Column 1*: centre of luminosity bin. *Column 2*: bivariate FIR luminosity function and its error. *Column 3*: number of galaxies in the bin. The numbers are not integers, due to the survival analysis applied.

4.4. $L_{\rm FIR}$ and L_B

Figure 7 plots $L_{\rm FIR}$ vs. L_B for the optically complete sample defined in Sect. 4.1. L_B was calculated as $L_B = 10^{(1.95-0.4 M_{\rm zw-corr})}$ in units of solar bolometric luminosity, where $M_{\rm zw-corr}$ is the absolute Zwicky magnitude corrected for systematic errors, Galactic extinction, internal extinction, and with K-correction applied (see Sect. 4.1 and Paper I). This definition[2] provides an estimate of the blue luminosity (νL_ν) at 4400 Å. In Fig. 7 we see scatter due to measurement uncertainties and intrinsic dispersion.

[2] Note that this definition differs by a factor of 1.7 from the definition used in Paper I, which was normalised to the solar luminosity in the blue.

Table 6. Correlation analysis of $L_{\rm FIR}$ vs. L_B.

(1) Sample	(2) n	(3) $n_{\rm up}$	(4) *Slope* (bisector)	(5) *Intercept* (bisector)	(6) *Slope* (L_B indep.)	(7) *Intercept* (L_B indep.)
Total	701	312	1.41 ± 0.02	−4.55 ± 0.25	1.11 ± 0.03	−1.57 ± 0.34
Sa–Sab (1–2)	49	18	1.37 ± 0.09	−4.29 ± 0.87	0.87 ± 0.23	0.76 ± 1.67
Sb–Sc (3–5)	452	181	1.35 ± 0.03	−3.98 ± 0.31	1.04 ± 0.06	−0.77 ± 0.57
Scd–Im (6–10)	115	49	1.25 ± 0.03	−2.99 ± 0.30	1.16 ± 0.05	−2.09 ± 0.58
Interacting	14	2	1.52 ± 0.12	−5.25 ± 1.15	1.43 ± 0.13	−4.34 ± 1.32

The slope and intercept are defined as: $\log(L_{\rm FIR}) = \log(L_B) \times slope + intercept$. The entries are: *Column 1*: subsamples considered. All subsamples are selected from the optically complete, magnitude limited subsample (see Sect. 4.1). In the early-type subsamples (E and S0), the relative number of undetected galaxies in $L_{\rm FIR}$, is very high so that a regression slope could not be determined. *Column 2*: total number of galaxies in the respective samples. *Column 3*: number of galaxies with upper limits in FIR. *Column 4*: bisector slope and its error of the best-fit regression line derived with the Schmitt binning method in the ASURV package. *Column 5*: bisector intercept. *Column 6*: slope and its error of the best-fit regression line derived with the Schmitt binning method in the ASURV package adopting L_B as independent variable. *Column 7*: bisector intercept adopting L_B as independent variable.

The latter should be minimised as much as possible to nature-driven dispersion. In this sample we have reduced dispersion due to both one-on-one interactions and environmental density. Most galaxies lie close to the correlation with a dispersion of 0.23 for the detected galaxies. There are four clear outliers close to $L_{\rm FIR} = 10^{11} L_\odot$. Three of them have been classified as possibly interacting in Paper II.

We applied linear regression analysis to estimate the functional relationship between the two variables. Since we are interested in the physical relation between the two, and since both have intrinsic uncertainties, we decided to use a symmetric method. We derived the regression coefficients for both $L_{\rm FIR}$ vs. L_B and L_B vs. $L_{\rm FIR}$ using ASURV and calculated the bisector regression line shown in Fig. 7 from these, following the formula in Isobe et al. (1990). We used the Schmitt's binning method (Schmitt 1985) as the only method offered by ASURV able to deal with censored data in the independent variable. We note, however, that for the cases where the other two methods (the estimation-maximisation method and the Buckley-James method) could be applied, a satisfactory agreement was found. The results for the linear regression (ASURV bisector) are listed in Table 6. The alternate approach would be to compute the regression assuming that optical luminosity is the independent variable. The results are also listed in Table 6 and show that the conclusions drawn in the following would not be substantially changed if L_B had been adopted as the independent variable. The best-fit slope for the entire sample is $L_{\rm FIR} \propto L_B^{1.41\pm0.02}$. Our slope is shallower than the one found by Perea et al. (1997) for a smaller subsample of the CIG, $L_B \propto L_{\rm FIR}^{0.65\pm0.09}$ (giving a slope of the inverse relation of $L_{\rm FIR} \propto L_B^{1.54}$). The main reason for this difference is our use of the bisector slope, whereas Perea et al. (1997) derived the slope with $L_{\rm FIR}$ as the independent variable. With our larger sample we derive a similar slope when adopting $L_{\rm FIR}$ as the independent variable ($L_B \propto L_{\rm FIR}^{0.55\pm0.03}$). For the present data set, however, we think that the bisector slope (or L_B as independent variable) is the better choice for investigating the functional relation between both variables. A possible explanation for the slope >1, suggested by Perea et al. (1997), is an increase of the dust extinction with galaxy luminosity, yielding a faster increase of the FIR emission in comparison to the extinction-affected blue luminosity. An alternative reason could be the increase of the recent star formation (SF) activity (traced by $L_{\rm FIR}$) with galaxy luminosity.

Figure 8 presents $L_{\rm FIR}$ vs. L_B for subsamples of different Hubble types. Due to the low detection rate for early-type galaxies (E–S0), no reliable regression fit could be derived for this subsample. The correlation for the early types shows evidence for a composite population with typical FIR deficient galaxies below the superimposed regression line and overluminous galaxies, showing a roughly linear correlation spanning 2 dex, above the line. As mentioned before, IR overluminous early-type galaxies must be regarded with suspicion until their morphologies are confirmed with higher resolution images than the POSS2 used for our morphology revision. At the same time, bona fide isolated early-types are of particular interest in view of ideas that see all of them as a product of nurture (mergers/stripping/harassment). There are only small differences in the measured slopes (see Table 6 and Fig. 8) of least-squares regression lines as a function of Hubble type.

Finally, we derive the distribution and the mean value of $R = \log(L_{\rm FIR}/L_B)$, a variable frequently used as an indicator of SF activity. In Table 4 we list the average and median values of R, together with those of $L_{\rm FIR}$ and L_B derived for different subsamples. Figure 9 shows R as a function of the morphological subtypes. No clear trend of $\langle R \rangle$ is found within the spiral galaxies with $\langle R \rangle$ essentially constant between T = 1–7 (Sa–Sd). $\langle R \rangle$, as well as $\langle L_{\rm FIR} \rangle$ (Fig. 5), is significantly lower for early types (E and S0), although values derived using survival analysis might be uncertain due to the large number of upper limits. This means that early-type galaxies have a lack in FIR emission with respect to their blue luminosity, with the ones showing values similar to spirals possibly being misclassified spirals. Late-type galaxies (Sd–Im) are on average less luminous both in $L_{\rm FIR}$ and L_B, but show the same $\langle R \rangle$ as spirals.

4.5. IRAS colours

IRAS flux ratios provide another potentially useful diagnostic. F_{60}/F_{100} (Telesco et al. 1988), F_{25}/F_{60} (XS91), and F_{12}/F_{25} (Bushouse et al. 1988) have been used as environmental diagnostics. For example, F_{60}/F_{100} measures the dust temperature and has been found to increase with the level of star formation activity (de Jong et al. 1984). F_{25}/F_{60} is an indicator for AGN activity, with values above $F_{25}/F_{60} = 0.3$ regarded as indicative of a Seyfert nucleus (de Grijp et al. 1985).

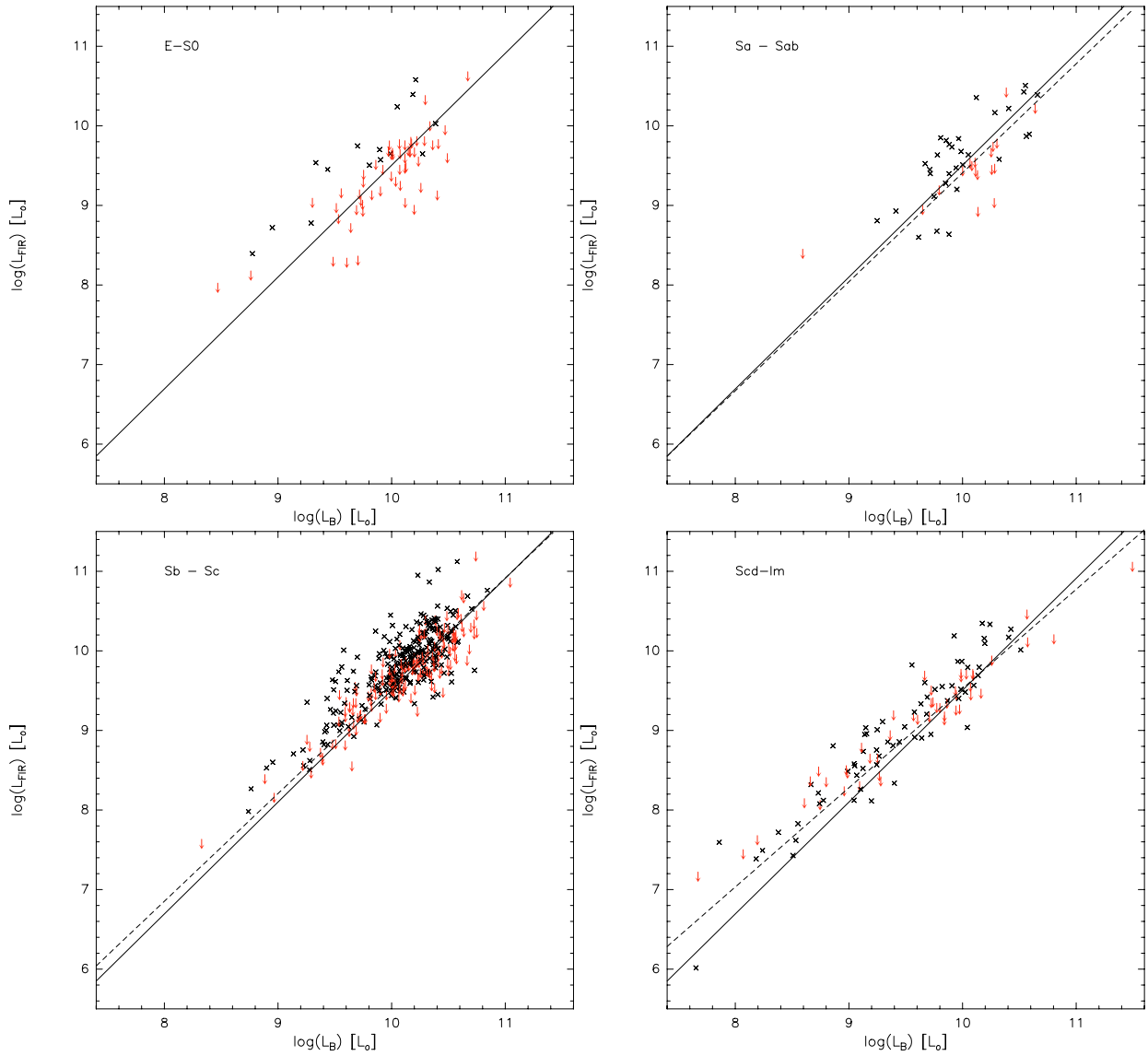

Fig. 8. $L_{\rm FIR}$ versus L_B for subsamples of different Hubble types. The full line is the bisector fit for the total AMIGA sample presented in Fig. 7, whereas the dashed line is the bisector fit for the present subsample. For the early type subsample (E and E–S0a), no reliable regression fit could be derived due to the large number of upper limits.

Figure 10 presents histograms of different IRAS colours for our optically complete subsample. The average and median values are listed in Table 7. The flux ratios $\log(F_{60}/F_{100})$ and $\log(F_{12}/F_{25})$ show a relatively symmetric distribution around the peak values. On the other hand, $\log(F_{25}/F_{60})$ exhibits a tail towards high values. The relative intensity of this tail weakens when only including detections with a higher S/N (we used $S/N > 7$ as a test), suggesting that part of it might be due to uncertain values, mainly at 25 μm. Another possible reason for high values of F_{25}/F_{60} can be the presence of AGNs, following the finding of de Grijp et al. (1985) that galaxies with $F_{25}/F_{60} > 0.3$ are very likely to host an AGN. We have checked the values of F_{25}/F_{60} for galaxies with an AGN listed in Sabater et al. (in prep.). Their list includes galaxies catalogued to have an AGN in NED or in the Véron-Cetty Catalogue of Quasars and Active Nuclei (Véron-Cetty & Véron 2003), as well as radio-excess galaxies with radio luminosities more than 5 times the values predicted by the radio-FIR correlation, and which are likely to be radio-loud quasars (Sopp & Alexander 1991). We found that 10 out of 11 active galaxies with detections at both 25 μm and 60 μm have values of $\log(F_{25}/F_{60}) \geq -0.7$, the value where the departure from symmetry in the distribution of F_{25}/F_{60} starts to be noticeable. Furthermore, 10 out of 14 galaxies with upper limits at F_{25} might lie above this threshold, but the upper limit at F_{25} makes a firm conclusion impossible. Thus, even though the absolute number of galaxies with known AGNs is not enough to explain the tail towards high F_{25}/F_{60}, they might be responsible for part of it.

In Fig. 11 we show the different IRAS colours as a function of Hubble type and in Table 7 we list the average and mean values. We notice the following:

- The range in $\log(F_{60}/F_{100})$ occupied by most galaxies is quite narrow, with almost all objects having $-0.7 \lesssim \log(F_{60}/F_{100}) \lesssim -0.2$.
- For $\log(F_{60}/F_{100})$, we find a clear trend with Hubble type. The value is highest for ellipticals (type −5), decreasing towards spirals and increasing again for late-type galaxies, starting from type 7–8, until irregulars (type 10).
- There is no significant trend in Hubble type visible for $\log(F_{25}/F_{60})$ or $\log(F_{12}/F_{25})$. The low number of detections

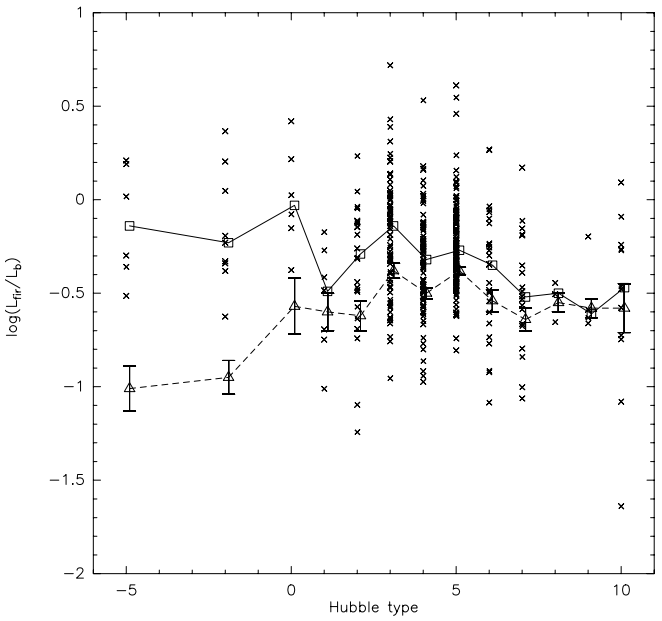

Fig. 9. $R = \log(L_{\rm FIR}/L_B)$, for the optically complete sample as a function of Hubble type. Only detections are shown. The open triangles give the mean value for each Hubble type, calculated with ASURV, taking the upper limits into account. The open squares are the median values for the detections.

might be the reason. No trend was found for $\log(F_{12}/F_{60})$ (not shown here) either, for which we derived a mean value for the total sample of -1.13 ± 0.02, and very similar values for each Hubble type individually.

5. Discussion

5.1. Comparison to other non-interacting samples

5.1.1. $L_{\rm FIR}$ and L_B

We compare the distribution of the FIR luminosity and of R to that of the galaxy sample of the Center of Astrophysics (CfA, Huchra et al. 1983), whose FIR properties, based on data of the IRAS FSC, were studied in Thuan & Sauvage (1992) (hereafter TS92) and Sauvage & Thuan (1992) (hereafter ST92). The CfA sample consists of 2445 galaxies representing a complete flux-limited sample ($m_{\rm zw} \leq 14.5$) selected in Galactic coordinates. No selection with respect to environment was carried out. To properly compare the two data sets, we applied the same magnitude cutoff as in TS92 ($m_{\rm zw} \leq 14.5$, in *uncorrected* Zwicky magnitudes) to our sample. We then compared the velocity distribution of these two samples (the CfA sample and our adapted sample) and found a very good agreement, with only two differences: In the CfA sample, the peak at ~5000 km s^{-1} is missing due to their restriction in coordinates which avoids the region of the Perseus-Pisces supercluster responsible for this peak. Furthermore, in our sample with the above magnitude restriction, there were no galaxies beyond 8500 km s^{-1}, whereas about 4% of the galaxies in the CfA sample have velocities above this value. We checked the effect of excluding these high velocity galaxies in the CfA sample on the subsequent results and did not notice any significant differences.

To correctly compare the luminosity distributions, we derived the distances for the CfA sample in the same way as for our galaxies: for close-by galaxies ($V_{\rm hel} < 1000$ km s^{-1}) (for which we used redshift-independent distances from the literature), we adopted the distances given by TS91, who used a Virgo-infall model to calculate them. For galaxies with $V_{\rm hel} > 1000$ km s^{-1}, we calculated the velocities after the 3K correction, $V_{\rm 3K}$, in the same way as for the AMIGA sample (see Paper I), and derived the distances as $D = V_{\rm 3K}/H_0$. We used the same Hubble constant ($H_0 = 75$ km s^{-1} Mpc^{-1}) in both samples.

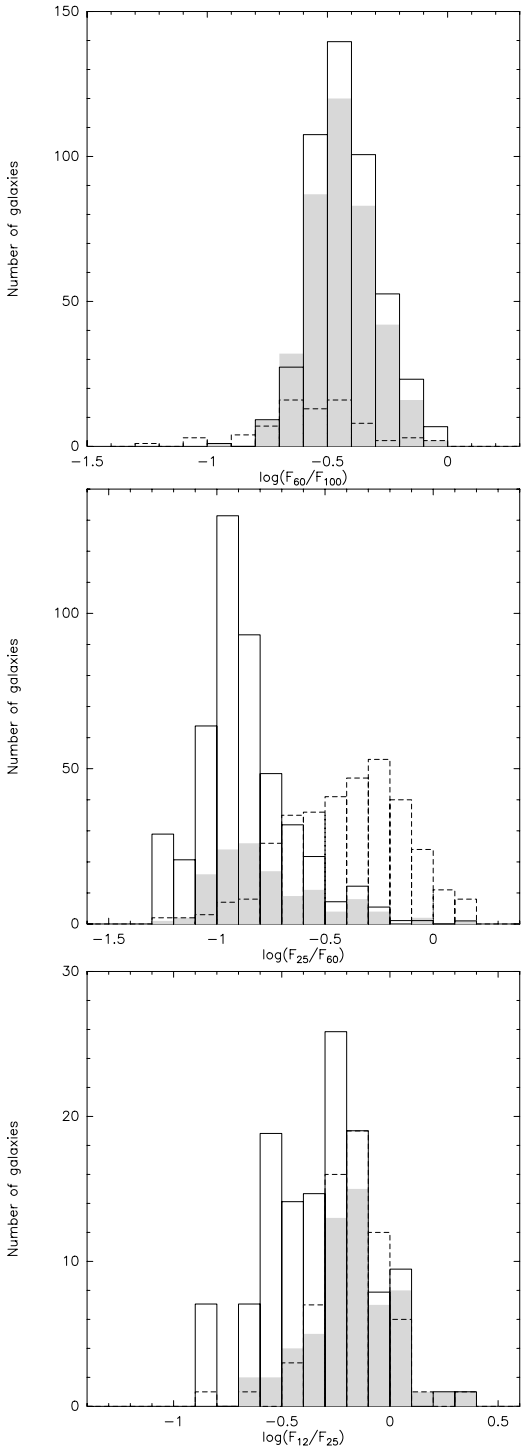

Fig. 10. IRAS colours for the AMIGA sample. The full line shows the histogram calculated with ASURV, taking into account censored data points, the grey-shaded area shows the detections, and the dashed line the upper limits. Only galaxies with detections at 60 μm are considered for $\log(F_{60}/F_{100})$ and $\log(F_{25}/F_{60})$, and only galaxies with detections at 25 μm for $\log(F_{12}/F_{25})$.

Table 7. Mean and median values of IRAS colours.

(1) Sample	(2) $n_{\rm tot}$	(3) $n_{\rm up}$	(4) $\langle\log(F_{60}/F_{100})\rangle$ med$(\log(F_{60}/F_{100}))$	(5) $n_{\rm up}$	(6) $\langle\log(F_{25}/F_{60})\rangle$ med$(\log(F_{25}/F_{60}))$	(7) $n_{\rm tot}$	(8) $n_{\rm up}$	(9) $\langle\log(F_{12}/F_{25})\rangle$ med$(\log(F_{12}/F_{25}))$
Total	468	76	-0.42 ± 0.01	343	-0.87 ± 0.02	126	67	-0.33 ± 0.03
			-0.45		-0.83			-0.18
S/Im (T = 1–10)	443	72	-0.43 ± 0.01	326	-0.87 ± 0.02	118	65	-0.33 ± 0.03
			-0.45		-0.83			-0.16
E (−5)	9	3	-0.23 ± 0.06	4	-0.73 ± 0.09	5	2	-0.47 ± 0.07
			-0.23		-0.74			-0.48
S0 (−2)	10	1	-0.39 ± 0.06	8	-1.02 ± 0.004	2	0	-0.16 ± 0.01
			-0.35		-1.02			-0.16
S0a (0)	6	0	-0.36 ± 0.07	5	-0.98^*	1	0	-0.27^*
			-0.27		-0.98			-0.27
Sa (1)	9	2	-0.43 ± 0.04	7	-0.79 ± 0.05	2	1	-0.32^*
			-0.42		0.71			-0.32
Sab (2)	27	3	-0.42 ± 0.03	18	-0.81 ± 0.04	9	4	-0.39 ± 0.09
			-0.45		-0.72			-0.22
Sb (3)	88	15	-0.41 ± 0.02	63	-0.87 ± 0.03	25	17	-0.50 ± 0.10
			-0.44		-0.89			-0.18
Sbc (4)	104	17	-0.45 ± 0.01	77	-0.83 ± 0.03	27	15	-0.27 ± 0.04
			-0.46		-0.78			-0.15
Sc (5)	138	24	-0.46 ± 0.01	107	-0.87 ± 0.03	32	14	-0.24 ± 0.05
			-0.48		-0.88			-0.10
Scd (6)	34	6	-0.45 ± 0.02	24	-0.87 ± 0.06	10	6	-0.36 ± 0.08
			-0.44		-0.82			-0.17
Sd (7)	21	2	-0.39 ± 0.03	13	-0.85 ± 0.07	8	5	-0.23 ± 0.003
			-0.40		-0.79			-0.23
Sdm (8)	4	1	-0.40 ± 0.02	3	-0.70 ± 0.15	1	1	–
			-0.40		-0.34			–
Sm (9)	5	1	-0.27 ± 0.02	3	-1.19 ± 0.08	2	1	-0.28 ± 0.04
			-0.28		-1.24			-0.22
Im (10)	13	1	-0.31 ± 0.03	11	-0.95 ± 0.08	2	1	-0.09 ± 0.10
			-0.35		-0.80			0.06
Interacting	14	2	-0.36 ± 0.03	10	-0.87 ± 0.03	4	0	-0.32 ± 0.08
			-0.39		-0.89			-0.34

For the entries marked with "*" ASURV was not able to calculate an error. A "–" means that the entry could not be calculated due to the low number of detections. For ratios involving F_{60}, only galaxies with detections at 60 μm are taken into account, and for $\log(F_{12}/F_{25})$, only galaxies with detections at 25 μm. The entries are: *Column 1*: considered subsample. All subsamples are selected from the optically complete, magnitude limited subsample. The interacting subsample consists of galaxies excluded from the CIG in Paper II (see Sect. 4.1). *Columns 2, and 7*: total number of galaxies in the subsample. *Columns 3, 5, and 8*: number of galaxies with upper limits. *Columns 4, 6, and 9*: first row: mean value of the ratio, using the Kaplan-Maier estimator from ASURV. Second row: median value of the same ratio, only for detections.

As a test to find possible systematic differences, we compared the distances, $L_{\rm FIR}$, L_B, and R for those galaxies that are common in both samples (total: n = 98, with FIR detections in both samples: n = 87). TS92 used B_T^0 to derive L_B. For the CfA sample, we estimated the corrected Zwicky magnitudes from B_T^0 using the linear relation found between both quantities in Paper I. Then we calculated L_B with the same formula as for the AMIGA sample. The calculation of $L_{\rm FIR}$ was also done in the same way for both samples. For the 98 galaxies, we found an excellent correlation between the distances used by us and those based on data of TS92, with a correlation coefficient of 0.995 and a slope of 1.01 ± 0.01. We also found a very good correlation between our values of $L_{\rm FIR}$ and the values derived by TS92 (correlation coefficient of 0.96 for detections), as well as for L_B (correlation coefficient of 0.90) and for R (correlation coefficient of 0.85 for detections). The mean values of $\log(L_{\rm FIR})$, $\log(L_B)$, and R for the galaxies in common practically agree (see Table 8), showing that a comparison of both data sets is justified.

In Fig. 12 we show a comparison of our distribution of $\log(L_{\rm FIR})$ to that of the CfA sample. Above $\log(L_{\rm FIR}/L_\odot) = 10.2$, a clear excess of CfA galaxies in comparison to our sample is visible. In Table 8 we list the mean values. The difference between the mean value of $\log(L_{\rm FIR})$ of the AMIGA and the CfA sample is 0.21–0.26 (with and without taking into account upper limits), which is a difference of 3–4σ. We performed statistical two-sample tests in the package ASURV and found that the two distributions were different, with a probability between 97.22% (Logrank test) and 99.87% (Gehan's Generalised Wilcoxon Test). The maximum probability increases to >99.95%, when only detections are taken into account. We also performed a Kolmogoroff-Smirnoff test on the detected data points and derived a probability of more than 99.75% that the mean values of $L_{\rm FIR}$ are different. Therefore, there is strong statistical evidence that the AMIGA sample has a lower $L_{\rm FIR}$ than the CfA sample, which is comparable, but not selected with respect to the environment. This suggests that the FIR luminosity is a variable driven by interaction.

The comparison of the distribution of R is shown in Fig. 13. We notice that the mean value of R is higher for the CfA sample than for the AMIGA sample. The difference is 0.12−0.14 (with and without upper limits) (see Table 8), which corresponds to 4−7σ. This difference has its origin in the higher value for $L_{\rm FIR}$ of the CfA sample, as the mean values for L_B are very similar (see Table 8), and the distribution of L_B for both samples

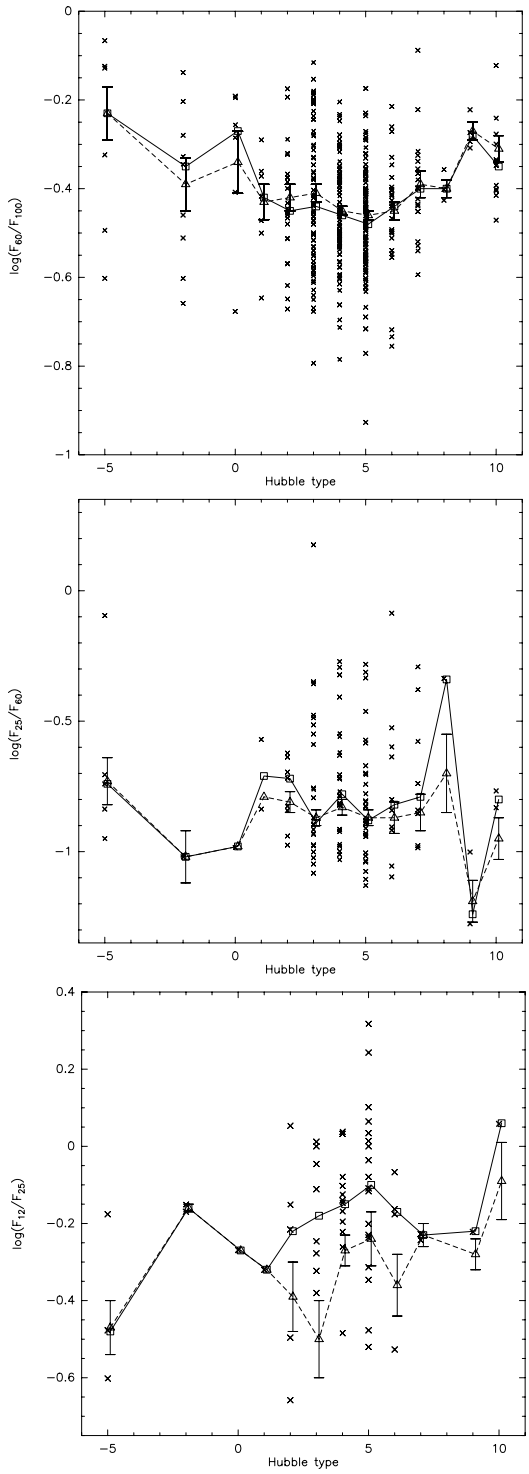

Fig. 11. IRAS colours as a function of Hubble type for the optically complete sample. For $\log(F_{60}/F_{100})$, and $\log(F_{25}/F_{60})$, only galaxies with detections at 60 μm are taken into account, and for $\log(F_{12}/F_{25})$, only galaxies with detections at 25 μm. Only detected galaxies are plotted (crosses). The open squares indicate the mean values from Table 7, calulated with ASURV and taking into account censored data points. The open triangles indicate the median values based on detections only. When no error bar is given, this could not be calculated due to the low number of detections.

(not shown here) practically agrees. We performed the statistical two-sample tests in the package ASURV and found that the two distributions of R were different with a probability between 97.3% (Logrank test) and >99.95% (Gehan's Generalised Wilcoxon Test). On the other hand, the tests showed that the distributions of L_B were identical with a non-negligible probability (28−68%) confirming that the difference in R has its origin in $L_{\rm FIR}$. Performing a Kolmogoroff-Smirnoff test on the detected data confirmed these results, yielding a probability of more than 99.999% that the mean values of R are different.

5.1.2. IRAS colours

We compared the distribution of the IRAS colours to the results found for the IRAS Bright Galaxy Sample (BGS, Sanders et al. 2003). The value of $\log(F_{60}/F_{100})$ of the BGS is higher by about 0.2–0.3 with respect to our sample. This is not surprising, since the BGS contains galaxies in a more active star-forming phase than the CIGs. The peaks of the distribution of the other colours in the BGS are very similar to ours, the only exception being the asymmetric tail towards high values of F_{25}/F_{60}, which is absent in the BGS.

A comparison to the results of XS91 for a smaller subsample of CIG galaxies (see Table 9) shows an excellent agreement of the values for $\log(F_{60}/F_{100})$ and $\log(F_{12}/F_{25})$. Our value for $\log(F_{25}/F_{60})$ is, however, slightly higher than that of XS91. We also compared our results to the CfA sample studied by ST92. For this aim, we again produced a different subsample, carrying out the same magnitude cut (<14.5 in uncorrected Zwicky magnitude) as in ST92. We found a very good agreement for $\log(F_{60}/F_{100})$ (see Table 9) and for $\log(F_{12}/F_{25})$. With respect to $\log(F_{25}/F_{60})$, we derived a slightly higher value for our sample. However, we consider the significance of this difference low due to the large number of upper limits.

In their analysis, ST92 found the same trend with Hubble type for $\log(F_{60}/F_{100})$ as we did. The value that they found for ellipticals, $\log(F_{60}/F_{100}) = -0.38$, is slightly higher than ours, whereas their value for irregulars, $\log(F_{60}/F_{100}) = -0.32$, agrees very well. Also, their values for spirals (between −0.45 and −0.47 for $T = 2$–5) are very close to ours. They explained the high F_{60}/F_{100} ratio in ellipticals by the concentration of the dust in the central regions where the radiation field is high, producing a higher dust temperature in this way. A high F_{60}/F_{100} ratio for irregulars has been found in other studies as well (e.g., Melisse & Israel 1994) and can be understood as a lack of "cirrus" emission with respect to FIR emission from H II regions.

5.2. Comparison to interacting galaxies

5.2.1. $L_{\rm FIR}$ and L_B

One of the motivations for refining and studying a large sample of isolated galaxies is to better define a baseline against which effects of environment could be quantified. Both mean IR diagnostic measures and their dispersion are of interest in this context. AMIGA began with a CIG sample selected to avoid near neighbours as much as possible. Yet visual reevaluation of the optical morphologies for the sample using POSS2/SDSS revealed 32 objects with clear signs of interaction (Paper II). These galaxies have been excluded from the present effort to characterise the isolated sample but offer a useful internal comparison sample to measure the sensitivity of the IR diagnostics to environment. Fourteen of these 32 galaxies have IRAS measures and apparent magnitudes between 11 and 15. Table 4 shows that the mean $\log(L_B)$ is almost identical to the isolated sample, while $\log(L_{\rm FIR})$ is brighter by ∼0.7 (0.6, when comparing to the

Table 8. Comparison to the CfA sample (Thuan & Sauvage 1992).

(1) Subsample	(2) n	(3) $\langle\log(L_B)\rangle$	(4) σ_B	(5) $n_{\rm up}$	(6) $\langle\log(L_{\rm FIR})\rangle$	(7) $\sigma_{\rm FIR}$	(8) $\langle\log(R)\rangle$	(9) σ_R
Total subsamples								
AMIGA (all)	207	9.80 ± 0.05	–	28	9.16 ± 0.09	–	−0.56 ± 0.03	–
AMIGA (det.)	179	9.83 ± 0.04	0.56	0	9.38 ± 0.05	0.71	−0.45 ± 0.02	0.31
CfA (TS92) (all)	1544	9.89 ± 0.01	–	210	9.42 ± 0.02	–	−0.44 ± 0.02	–
CfA (TS92) (det.)	1334	9.89 ± 0.01	0.54	0	9.59 ± 0.02	0.73	−0.31 ± 0.01	0.41
Galaxies in common								
AMIGA(all)	98	9.82 ± 0.06	–	4	9.37 ± 0.07	–	−0.43 ± 0.03	–
AMIGA (det.)	87	9.84 ± 0.06	0.55	0	9.44 ± 0.07	0.66	−0.40 ± 0.03	0.29
CfA (TS92) (all)	98	9.85 ± 0.05	–	7	9.37 ± 0.07	–	−0.47 ± 0.04	–
CfA (TS92) (det.)	87	9.85 ± 0.05	0.50	0	9.43 ± 0.07	0.62	−0.42 ± 0.04	0.33

The entries are: *Column 1*: sample considered. Both samples are selected with the same magnitude limit of (uncorrected) $m_{\rm zw} \leq 14.5$. The distances of the galaxies of the CfA sample have been derived in the same way as for the AMIGA sample (see Sect. 5.1.1). We give both the results obtained with ASURV (first row) and the results with detections only (second row). *Column 2*: total number of galaxies. *Column 3*: mean value of $\log(L_B)$ and its error. *Column 4*: standard deviation of $\log(L_B)$. *Column 5*: number of galaxies with upper limits in $L_{\rm FIR}$. *Column 6*: mean value of $\log(L_{\rm FIR})$ and its error. *Column 7*: standard deviation of $\log(L_{\rm FIR})$. *Column 8*: mean value of $R = \log(L_{\rm FIR}/L_B)$ and its error. *Column 9*: standard deviation of $\log(L_{\rm FIR}/L_B)$.

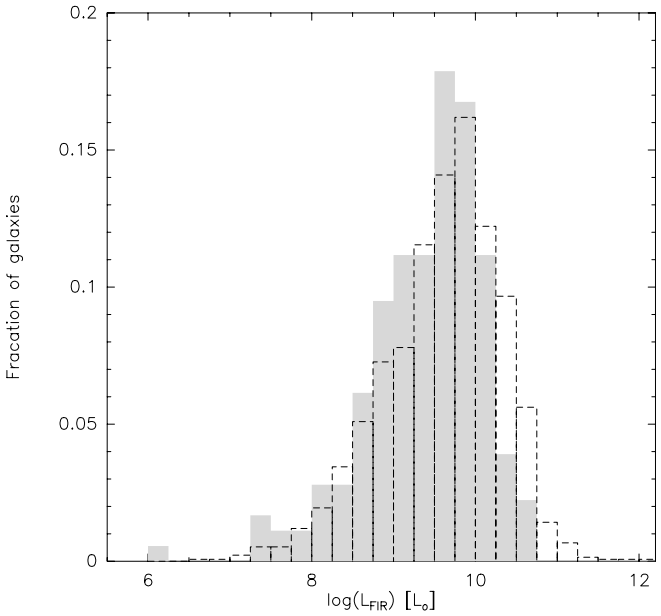

Fig. 12. The percentage FIR luminosity distribution for the FIR detections in the AMIGA sample restricted to (uncorrected) $m_{\rm zw} \leq 14.5$ (shaded area) and the corresponding distribution for the CfA sample (dotted line).

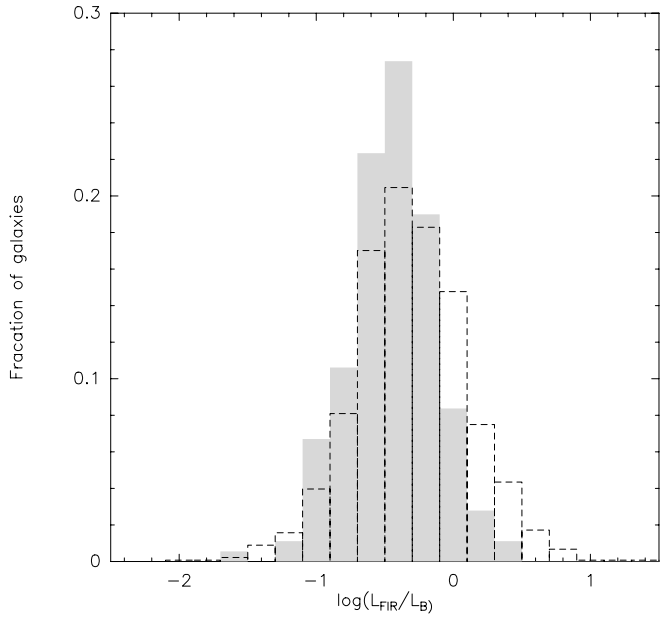

Fig. 13. The percentage distribution of $R = \log(L_{\rm FIR}/L_B)$ for the FIR detections in the AMIGA sample restricted to (uncorrected) $m_{\rm zw} \leq 14.5$ (shaded area) and the corresponding distribution for the CfA sample (dotted line).

spiral/irregular subsample). Similarly, the mean FIR-to-optical flux ratio, $\langle R\rangle$, is 0.50 (0.43 for the spiral/irregular subsample) higher. This shows that there is a significant difference in R between isolated and interacting galaxies due to an enhancement in $L_{\rm FIR}$ of the latter.

Figure 14 shows the correlation between $L_{\rm FIR}$ and L_B for this interacting subsample. Regression analysis yields a steeper slope (see Table 6), as is usually found for interacting samples, indicating that $L_{\rm FIR}$ increases faster as a function of L_B in comparison to the non-interacting sample. The reason for this FIR excess is most likely an enhancement of (dust-enshrouded) SF in interacting galaxies. This is consistent with the results in Perea et al. (1997), where a FIR enhancement was found for a sample of perturbed galaxies. We included their weakly and strongly interacting samples in Fig. 14. The effect is strongest for their strongly perturbed sample. The average FIR excess (i.e., average deviation from the AMIGA regression line) for the strong and weak interacting samples are 0.87 and 0.49, respectively.

XS91 compared mean FIR-to-optical flux ratios and found a much smaller, but significant, difference between spiral-spiral pairs ($R = -0.17$) and a late-type subsample from the CIG ($R = -0.30$). The difference increased when considering only close pairs ($R = -0.02$). To compare their result to ours, we have to take into account that they used *uncorrected* Zwicky magnitudes. The correction that we applied (see Paper I) changed the Zwicky magnitudes by on average −0.67 magnitudes, corresponding to a change in R of −0.27 dex. Taking this into account, the value R for the CIG subsample of XS91 is practically the same as ours, whereas R for the pair sample in XS91 is below (∼0.2–0.4) the value of our interacting sample. Due to the small size of our interacting sample and the different selection

Table 9. Comparison of IRAS colours to other studies.

(1) Sample	(2) n/n_{up}	(3) $\langle\log(\frac{F_{60}}{F_{100}})\rangle$	(4) n/n_{up}	(5) $\langle\log(\frac{F_{25}}{F_{60}})\rangle$	(6) n/n_{up}	(7) $\langle\log(\frac{F_{12}}{F_{25}})\rangle$
Isolated samples						
AMIGA total	468/76	-0.42 ± 0.01	468/343	-0.87 ± 0.02	126/67	-0.33 ± 0.03
AMIGA, only det.	392/0	-0.44 ± 0.01	125/0	-0.76 ± 0.02	59/0	-0.18 ± 0.03
XS91 CIG	261/–	-0.42 ± 0.01	–	-0.96 ± 0.02	–	-0.32 ± 0.04
Bushouse et al. (1988) isolated	68/0	-0.39	–	–	34/0	-0.21
AMIGA $m_{zw(uncorr)} < 14.5$	183/4	-0.43 ± 0.01	183/90	-0.88 ± 0.02	93/35	-0.26 ± 0.03
AMIGA $m_{zw(uncorr)} < 14.5$, (det.)	179/0	-0.43 ± 0.01	93/0	-0.82 ± 0.02	58/0	-0.18 ± 0.02
CfA (ST92)	1465/131	-0.42 ± 0.004	1465/771	-0.94 ± 0.01	706/154	-0.26 ± 0.01
CfA (ST92), (det)	1330/0	-0.43 ± 0.004	694/0	-0.87 ± 0.01	552/0	-0.21 ± 0.01
Interacting samples						
AMIGA interacting	14/2	-0.36 ± 0.03	14/10	-0.87 ± 0.03	4/0	-0.32 ± 0.08
XS91 wide pairs	–	-0.39 ± 0.01	–	-0.93 ± 0.02	–	-0.52 ± 0.07
XS91 close pairs	–	-0.31 ± 0.01	–	-0.93 ± 0.02	–	-0.65 ± 0.08
Bushouse et al. (1988) inter.	98/0	-0.33	–	–	48/0	-0.42

The entries are: *Column 1*: sample considered. *Columns 2, 4, 6*: total number of galaxies and number of galaxies with upper limits. *Columns 3, 5, 7*: IRAS colour. For ratios involving F_{60}, only data points with detections at this wavelength were considered, whereas in $\langle\log(F_{12}/F_{25})\rangle$ only data points with detections at 25 μm were taken into account. A "–" means that the corresponding data point was not given in the reference.

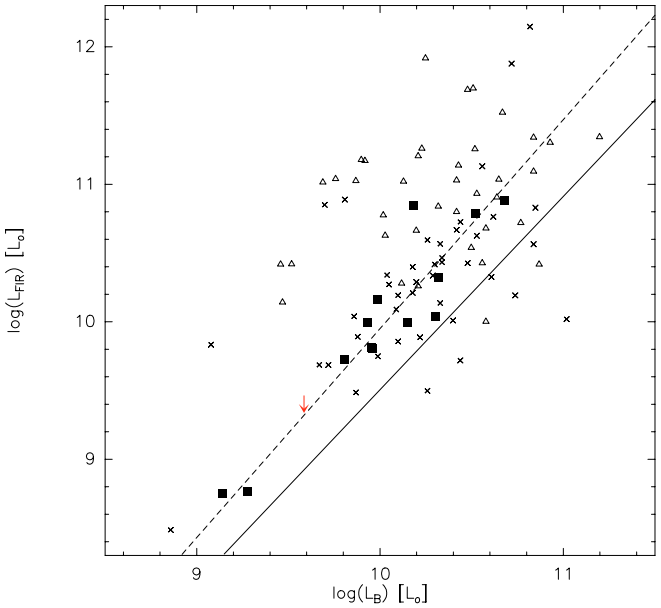

Fig. 14. L_{FIR} vs. L_B for various interacting subsamples. The filled squares and arrows denote the galaxies from the CIG, showing signs of interaction (see Paper II). The dashed line is the regression fit to this subsample. The triangles indicate strongly interacting galaxies, and the crosses weakly interacting galaxies from Perea et al. (1997). The full line is the fit to the total AMIGA sample (n = 701) of Fig. 7.

(the study of XS91 restricted the environmental signature to the effects of one-on-one interactions), we do not want to draw any conclusions from this difference.

5.2.2. IRAS colours

We found a slightly higher value of $\log(F_{60}/F_{100})$ for the possibly interacting galaxies in the CIG than for the total AMIGA sample (see Table 7). The difference is, however, only 2σ, and thus not statistically significant. In the other colours ($\log(F_{25}/F_{60})$, $\log(F_{12}/F_{25})$, or $\log(F_{12}/F_{60})$), we found, within the errors, no difference between both samples.

A trend of higher $\log(F_{60}/F_{100})$ values in interacting galaxies has been found in other studies (see Table 9). XS91 compared their subsample of CIGs to paired galaxies. They found a value very close to our interacting sample for wide late-type pairs (i.e., a distance between partners larger than the diameter of the primary) and an even higher value, significantly higher than for the value for the CIGs, for close late-type pairs (i.e., a distance between partners less than the diameter of the primary). Bushouse et al. (1988) studied the MIR/FIR properties of a sample of 109 colliding galaxies and compared it to more isolated galaxies from the sample of Kennicutt & Kent (1983). In their study, they only took into account IRAS detections. Their values for $\log(F_{60}/F_{100})$, both for the interacting as well as for the comparison sample, is in reasonable agreement with our study and that of XS91.

We did not find a significant difference in either F_{25}/F_{60} or F_{12}/F_{25} between isolated and interacting galaxies. In contrast to this, XS91 obtained a lower value for F_{12}/F_{25} both for the close and the wide pair samples. Bushouse et al. (1988) also found a higher value for F_{12}/F_{25} in the interacting sample, although their result has to be taken with caution because only detections were included (thereby skewing the result to higher values). Given the very low number of galaxies with detections in our interacting subsample, the significance of these differences is, however, not statistically meaningful.

5.3. Nature of the FIR brightest galaxies

MIR/FIR measures have been found to be sensitive diagnostics of enhanced SF. Since SF can be greatly enhanced by the presence of companions, we can ask if any of the most FIR luminous galaxies in our sample are really isolated. Naturally, as discussed in Paper II, we are limited in our ability to describe galaxy form and to detect close companions by the quality of the available images. Table 10 lists the FIR brightest galaxies (with $\log(L_{FIR}/L_\odot) > 10.5$) in our sample and the results of re-examination of POSS2 and other data sources for them. More than half of this sample are likely to involve interacting systems. A very few may represent the most luminous examples of self-induced star formation or the IR emission is dominated by a yet undetected active nucleus (many do not have published spectra).

Table 10. Galaxies with $\log(L_{\rm FIR}/L_\odot) > 10.5$.

(1) CIG	(2) $\log(L_{\rm FIR}/L_\odot)$	(3) Hubble type	(4) Comment
55	11.12	Sc ($T = 5$)	I/A + Sy/LINER
143	10.86	Sbc ($T = 4$)	I/A? lopsided spiral
148	10.56	Sbc ($T = 4$)	I/A
232	10.69	Sc ($T = 5$)	I/A?
302	11.02	Sc ($T = 5$)	I/A? peculiar
361	10.51	Sab ($T = 2$)	Isolated spiral?
444	10.54	Sb ($T = 3$)	Possibly Sm companion
709	10.53	Sc ($T = 5$)	Sm companion nearby
715	10.76	Sc ($T = 5$)	I/A
829	10.51	Sb ($T = 3$)	Blue Compact
841	10.58	S0 ($T = -2$)	large inclined S0
866	10.95	Sb ($T = 3$)	Isolated, LINER

The entries are: *Column 1*: CIG number. *Column 2*: FIR luminosity. *Column 3*: Hubble type. *Column 4*: comment after visual inspection of optical images, and consultation of NED. I/A means interacting, I/A?: possibly interacting, Sy: Seyfert galaxy.

CIG 709 epitomises another issue raised in Paper II. While it appears to be isolated from similarly sized objects, it shows striking structural asymmetries and a small companion about one diameter distant. It is still unclear whether such small companions are capable of significantly enhancing star formation and producing structural deformations in massive spirals (see also Espada et al. 2005).

We furthermore inspected the most extreme outliers from the regression fit between $L_{\rm FIR}$ and L_B. The outliers on the high side come under immediate suspicion as interactors that were missed in the morphology survey. Only two show $\log(L_{\rm FIR}) > 11.0$, and both are possible interacting systems – in NED they are described as Seyfert/LINER (CIG 55), and H II galaxy (CIG 302). Several others are candidate interactors or have an active nucleus. Galaxies falling below the regression are either early-types (E and S0), known to be deficient in FIR emission, or highly inclined galaxies. The internal extinction correction for such objects is large and uncertain, suggesting that the low $L_{\rm FIR}/L_B$ measures may be due to overcorrection of the blue magnitude.

6. Conclusions

We present a MIR/FIR analysis of a sample of the most isolated galaxies in the local universe, obtained from the Catalogue of Isolated Galaxies (CIG). This analysis is part of our multi-wavelength study of the properties of the interstellar medium of this sample and involves ADDSCAN/SCANPI reprocessing of IRAS data for all 1030 galaxies (out of 1050 in the CIG) covered by IRAS. We increased the detection rate with respect to the PSC and FSC in all IRAS bands and present our AMIGA sample of 701 CIG galaxies as the best available control sample against which to evaluate the IR signatures of environment in local galaxy samples. Our sample is large enough to permit comparison of IR properties for galaxy morphology subclasses. Our main results are the following:

1. The galaxies in our sample have modest FIR luminosities, with only 14 objects (corresponding to <2% of the sample) above $\log(L_{\rm FIR}/L_\odot) = 10.5$. The mean $\log(L_{\rm FIR})$ of our sample is 3–4σ (0.21–0.26 dex) below the corresponding value for the CfA sample studied by TS92 and ST92, which is a sample of nearby galaxies similar to ours, but selected without considering the environment. In addition, a lower value (by 0.12–0.14 dex, corresponding to 4–7σ), compared to the CfA sample, was found for the mean $R = \log(L_{\rm FIR}/L_B)$ of our sample. This suggests that the FIR emission is a parameter driven by interaction and that our sample of isolated galaxies shows a value close to the lowest possible.
2. We find evidence for a systematic increase in FIR luminosity from type S0/a to Sc, followed by a decline for later types (dominated by dwarf galaxies), possibly reflecting lower dust masses in those galaxies or less efficient star formation. At the same time, R is essentially constant for all Hubble types later than S0/a, suggesting that the SF efficiency in isolated spirals and irregulars is roughly constant.
3. Early-type galaxies (E and S0) show a lower average R than the spirals. We can divide them into two populations: 1) undetected galaxies (the majority) with low upper limits in R and 2) a population of early types with $L_{\rm FIR}$ and R that are similar to spiral galaxies. The latter galaxies require confirmation of the assigned early-types. If real, they represent an interesting class of isolated galaxies.
4. We calculated the bivariate FIR luminosity function, which was found to be in good agreement with previous studies (XS91) based on a smaller subsample of the CIG. The FIRLF is dominated by moderately FIR luminous galaxies (only 3 objects have $\log(L_{\rm FIR}/L_\odot) > 11.0$) and is well described by a Schechter function. This contrasts to results obtained for FIR selected samples (e.g., Soifer et al. 1986; Sanders et al. 2003), where a double power law is needed to achieve a fit to the high-luminosity end of the FIRLF.
5. We found a correlation between $L_{\rm FIR}$ and L_B with a slope above 1 ($L_{\rm FIR} \propto {L_B}^{1.41}$) with only modest variations as a function of Hubble type. Possible reasons for the slope being >1 are an increase in extinction or an enhancement of the recent SF activity with galaxy luminosity.
6. We identified a small population of possibly interacting galaxies in the CIG (Paper II) and these show a significantly higher mean FIR luminosity than the rest of the sample. They lie above the regression line derived for our optically selected CIG sample. The same was found for samples of interacting galaxies from Perea et al. (1997). This suggests that the FIR emission is enhanced due to the interacting.
7. We found a trend of F_{60}/F_{100} with Hubble type: elliptical galaxies and irregular galaxies have a higher F_{60}/F_{100} than spirals, indicating a hotter dust temperature. For the ellipticals the most likely reason is the higher concentration of dust towards the inner regions of the galaxies (ST92), whereas in irregulars, a lack of cirrus emission is the most probable cause.
8. The value of F_{60}/F_{100} of the AMIGA sample was found to be lower than that of interacting samples from the literature (XS91 and Bushouse 1988), indicating that interaction can increase the dust temperature.

As the largest and most isolated sample in the local Universe, AMIGA can serve as a valuable control when assessing the effects of environment on other local samples of galaxies. This can, in turn, clarify our interpretation of the FIR signature in samples at higher redshift.

Acknowledgements. We would like to thank M. Sauvage for making the data of his sample available to us. This research has made use of the NASA/IPAC Extragalactic Database (NED), which is operated by the Jet Propulsion Laboratory, California Institute of Technology, under contract with the National Aeronautics and Space Administration, and of the Lyon Extragalactic Database

(LEDA). This work has been partially supported by DGI Grant AYA 2005-07516-C02-01 and the Junta de Andalucía (Spain). UL acknowledges support by the research project ESP 2004-06870-C02-02. J.S. is partially supported by a sabbatical grant SAB2004-01-04 of the Spanish Ministerio de Educación y Ciencias. GB acknowledges support at the IAA/CSIC by an I3P contract (I3P-PC2005F) funded by the European Social Fund.

References

Bertin, E., & Arnouts, S. 1996, A&AS, 117, 393
Bushouse, H. A. 1987, ApJ, 320, 49
Bushouse, H. A., Lamb, S. S., & Werner, M. W. 1988, ApJ, 335, 74
Bergvall, N., Laurikainen, E., & Aalto, S. 2003, A&A, 405, 31
de Jong, T., Clegg, P. E., Rowan-Robinson, M., et al. 1984, ApJ, 278, L67
de Grijp, M. H. K., Miley, G. K., Lub, J., & de Jong, T. 1985, Nature, 314, 240
Espada, D., Bosma, A., Verdes-Montenegro, L., et al. 2005, A&A, 442, 455
Feigelson, E. D., & Nelson, P. I. 1985, ApJ, 293, 192
Helou, G., Kahn, I. R., Malek, L., & Boehmer, L. 1988, ApJS, 52, 89
Hernquist, L. 1989, Nature, 340, 687
Hernandez Toledo, H. M., Dultzin-Hacyan, D., & Sulentic, J. W. 2001, AJ, 121, 1319
Hickson, P. 1982, ApJ, 255, 382
Huchra, J., Davis, M., Latham, D., & Tonry, J. 1983, ApJS, 52, 89
Isobe, T., & Feigelson, E. D. 1990, BAAS, 22, 917
Isobe, T., Feigelson, E. D., & Nelson, P. I. 1986, ApJ, 306, 490
Isobe, T., Feigelson, E. D., Akritas, M. G., & Babu, G. J. 1990, ApJ, 364, 104
Karachentseva, V. E. 1973, Comm. Spec. Ap. Obs., USSR, 8, 1
Karachentseva, V. E., Lebedev, V. S., & Shcherbanovskij, A. L. 1986, Catalogue of Isolated Galaxies. Bull. Inf. CDS, 30, 125
Kennicutt, R. C., & Kent, S. M. 1983, AJ, 88, 1094
La Valley, M., Isoble, T., & Feigelson, E. D. 1992, in ASP Conf. Ser. 25, ADASS I., ed. D. M. Worrall, C. Biemesderfer, & J. Barnes (San Francisco: ASP), 245
Leon, S., & Verdes-Montenegro, L. 2003, A&A, 411, 391
Melisse, J. P. M., & Israel, F. P. 1994, A&A, 285, 51
Nilson, P. 1973, Uppsala General Catalogue of Galaxies (UGC, Uppsala: Astronomiska Observatorium)
Perea, J., del Olmo, A., Verdes-Montenegro, L., & Yun, M. S. 1997, ApJ, 490, 166
Rice, W., Lonsdale, C. J., Soifer, B. T., et al. 1988, ApJS, 68, 91
Sauvage, M., & Thuan, T. X. 1992, ApJ, 429, 153 (ST92)
Sanders, D. B., Mazzarella, J. M., Kim, D.-C., Surace, J. A., & Soifer, B. T. 2003, AJ, 126, 1607
Schmitt, J. H. M. 1985, ApJ, 293, 178
Soifer, B. T., Sanders, D. B., Neugebauer, G., et al. 1986, ApJ, 303, L41
Sopp, H. M., & Alexander, P. 1991, MNRAS, 251, 14
Sulentic, J. W. 1976, ApJS, 32, 171
Sulentic, J. W., & Rabaca, C. R. 1994, ApJ, 429, 531
Sulentic, J. W., Verdes-Montenegro, L., Bergond, G., et al. 2006, A&A, 449, 937 (Paper II)
Telesco, C. M., Wolstencroft, R. D., & Done, C. 1988, ApJ, 329, 174
Thuan, T. X., & Sauvage, M. 1992, A&AS, 92, 749 (TS92)
Verdes-Montenegro, L., Yun, M. S., Perea, J., del Olmo, A., & Ho, P. T. P. 1998, ApJ, 497, 89
Verdes-Montenegro, L., Sulentic, J., Lisenfeld, U., et al. 2005, A&A, 436, 443 (Paper I)
Véron-Cetty, M.-P., & Véron, P. 2003, A&A, 412, 399
Xu, C., & Sulentic, J. W. 1991, ApJ, 374, 407 (XS91)
Zwicky, F., Herzog, E., Karpowicz, M., Kowal, C., & Wild, P. 1961–1968, Catalogue of Galaxies and of Cluster of Galaxies (CGCG, Pasadena: California Institute of Technology)